

A Novel Brain PET Radiotracer for Imaging Alpha Synuclein Fibrils in Multiple System Atrophy

Published as part of the Journal of Medicinal Chemistry virtual special issue "Diagnostic and Therapeutic Radiopharmaceuticals".

Ho Young Kim, Wai Kit Chia, Chia-Ju Hsieh, Dinahlee Saturnino Guarino, Thomas J. A. Graham, Zsofia Lengyel-Zhand, Mark Schneider, Cosette Tomita, Marshall G. Lougee, Hee Jong Kim, Vinayak V. Pagar, Hsiaoju Lee, Catherine Hou, Benjamin A. Garcia, E. James Petersson, Jennifer O'Shea, Paul T. Kotzbauer, Chester A. Mathis, Virginia M.-Y. Lee, Kelvin C. Luk, and Robert H. Mach*



Cite This: *J. Med. Chem.* 2023, 66, 12185–12202



Read Online

ACCESS |



Metrics & More

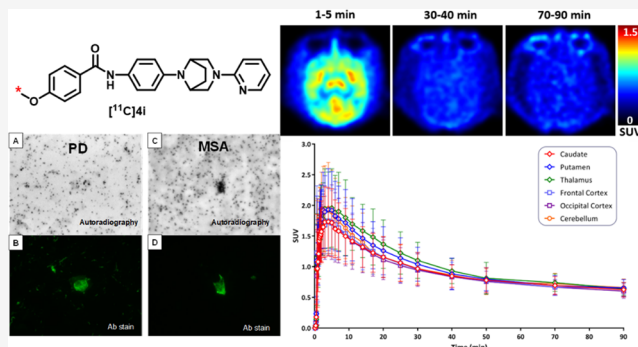


Article Recommendations



Supporting Information

ABSTRACT: Abnormal α -synuclein (α -syn) aggregation characterizes α -synucleinopathies, including Parkinson's disease (PD) and multiple system atrophy (MSA). However, no suitable positron emission tomography (PET) radiotracer for imaging α -syn in PD and MSA exists currently. Our structure–activity relationship studies identified 4-methoxy-*N*-(4-(3-(pyridin-2-yl)-3,8-diazabicyclo[3.2.1]octan-8-yl)phenyl)benzamide (**4i**) as a PET radiotracer candidate for imaging α -syn. *In vitro* assays revealed high binding of **4i** to recombinant α -syn fibrils (inhibition constant (K_i) = 6.1 nM) and low affinity for amyloid beta ($A\beta$) fibrils in Alzheimer's disease (AD) homogenates. However, [^3H]**4i** also exhibited high specific binding to AD, progressive supranuclear palsy, and corticobasal degeneration tissues as well as PD and MSA tissues, suggesting notable affinity to tau. Nevertheless, the specific binding to pathologic α -syn aggregates in MSA post-mortem brain tissues was significantly higher than in PD tissues. This finding demonstrated the potential use of [^{11}C]**4i** as a PET tracer for imaging α -syn in MSA patients. Nonhuman primate PET studies confirmed good brain uptake and rapid washout for [^{11}C]**4i**.



INTRODUCTION

Misfolded protein aggregates in the central nervous system (CNS) are pathological hallmarks of most neurodegenerative diseases.¹ Insoluble α -synuclein (α -syn) aggregates are a pathological feature of α -synucleinopathies, and its abnormal accumulations within the cytoplasm are commonly identified in patients with Parkinson's disease (PD), dementia with Lewy bodies (DLB), and multiple system atrophy (MSA).^{2,3} α -Synucleinopathies are categorized into two classes according to fibrillar α -syn inclusions bodies: (1) Lewy bodies (LBs) or Lewy neurites (LNs) and (2) Papp-Lanths bodies or glia cell inclusions (GCIs). In PD and DLB, α -syn aggregates form insoluble intraneuronal inclusions as LBs^{4,5} and LNs in axonal processes,⁶ whereas in MSA, GCIs, or Papp-Lanths bodies composed mainly of filamentous α -syn are found in oligodendrocytes.^{7–9} Previous studies demonstrated that these α -synucleinopathies possess distinct structural and biological properties.^{10–13}

Since aggregation of α -syn is apparently an early driver of the pathogenesis of PD and MSA, α -syn aggregates have been recognized as a suitable biomarker for imaging these α -

synucleinopathies.^{11,14–16} Positron emission tomography (PET) is an imaging modality that allows for the noninvasive visualization and quantification of various *in vivo* biological processes including altered target expressions using a radiotracer. The quantification of α -syn aggregates using PET in patients with α -synucleinopathies has the potential to serve as a valuable tool for early stage prognostic indications and evaluating disease-modifying therapeutics in slowing disease progression. The development of an α -syn radiotracer has been highly encouraged by the success of amyloid beta ($A\beta$)^{17–20} or tau^{21–24} PET probes for the diagnosis of Alzheimer's disease (AD). Particularly, tau-based neurofibrillary tangles (NFTs) occur in the later stage of disease progression with clinical

Received: April 30, 2023

Published: August 31, 2023



features while the deposition of $A\beta$ plaques precedes onset.²⁵ Similarly, early diagnosis of PD or MSA using an α -syn PET tracer would identify patients who could benefit most from α -syn therapeutic strategies currently under development. Despite the significance of detecting α -syn aggregates in PD or MSA patients, there is currently no clinical PET tracer available. [¹⁸F]ACI-12589, with a K_D value of 22–30 nM in MSA tissues, has been found to present distinct uptake in the cerebellar white matter or peduncles of MSA patients consistent with α -syn pathology.²⁶

There are several hurdles that make the development of an α -syn PET tracer difficult.²⁷ The first factor is binding affinity. Since the density of α -syn aggregates is much lower than those of $A\beta$ plaques or tau NFTs (approximately 1/10 to 1/50 versus $A\beta$), α -syn ligands are required to exhibit a high binding affinity for α -syn fibrils.^{28,29} Also, achieving binding selectivity for an aggregated α -syn ligand versus $A\beta$ or tau is very challenging due to the similar β -sheet-rich structure in each fibril.^{30–32} $A\beta$ pathology is observed in over 80% of total α -synucleinopathies (LBD and MSA),²⁹ so it is essential that an α -syn PET tracer should distinguish α -syn aggregates from $A\beta$ depositions. Furthermore, a successful α -syn PET tracer should have favorable physicochemical properties (e.g., MW, topological polar surface area (tPSA), LogD, etc.) for brain or cell membrane permeability, favorable metabolism leading to polar metabolites, and low nonspecific binding.³³

Numerous compounds targeting α -syn fibrils have been synthesized to date. For example, Borroni and colleagues disclosed in the patent literature radiolabeled *N*-phenylbenzamide analogs including [³H]BF2846 that involved different modifications of the structure except for the piperazine ring.³⁴ [³H]BF2846 and its congeners exhibited high binding affinity for α -syn in radioligand binding assays and *ex vivo* autoradiography studies ($K_D = 2.0$ nM for [³H]BF2846).²⁷ These analogs were also reported to have good target engagement, high brain penetration, and low nonspecific binding in brain. Molecular docking and photoaffinity labeling studies from our lab suggested that there are putative multiple binding sites within α -syn fibrils and [³H]BF2846 and its analogs bind to site 9 preferentially.³⁵ However, the use of ¹⁸F-labeled analogs of BF2846 for *in vivo* imaging PET studies is limited due to their high binding affinity for $A\beta$ fibrils.

In the current study, we performed a structure–activity relationship (SAR) investigation of BF2846 in which the piperazine ring has been replaced with different heterocyclic moieties including diazaspirocyclic or bridged amino cores (Figure 1). This strategy has been used by our group previously to reduce the off-target binding of dopamine D3 antagonists.³⁶ The results of our studies indicated that it is possible to prepare α -syn radioligands having a reduced affinity for $A\beta$ fibrils using this strategy. Our study also identified a novel radioligand that

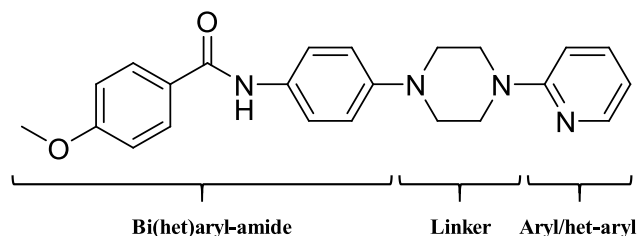


Figure 1. Chemical structure of lead compound, BF2846.

binds preferentially to α -syn fibrils in MSA versus PD brain samples using *in vitro* autoradiography in post-mortem brain samples.

RESULTS

Chemistry. The synthesis of the BF2846 analogs containing heterocyclic structures with varying sizes of diazaspirocyclic rings, as well as diazabridged rings, is illustrated in Scheme 1A. In addition, pyridine isomers were introduced for Ar₁ as a substitute for benzene attached to the amino core (Figure 2), potentially reducing the lipophilicity of the ligand for better brain uptake and pharmacokinetics. The common intermediates 1a–c were synthesized by the condensation of acyl chloride and aniline under basic conditions. Since the reaction for 1b prefers to form a diamide in which two 4-methoxybenzamide moieties are bound with one amino-pyridine, the additional 4-methoxybenzamide was cleaved using refluxing with K₂CO₃ in aqueous methanol to afford the desired amide, 1b, in quantitative yield. Although less diamide was found in the reaction to prepare 1c, the additional 4-methoxybenzamide was not removed under the same reaction conditions. However, the diamide could be separated from 1c using flash chromatography.

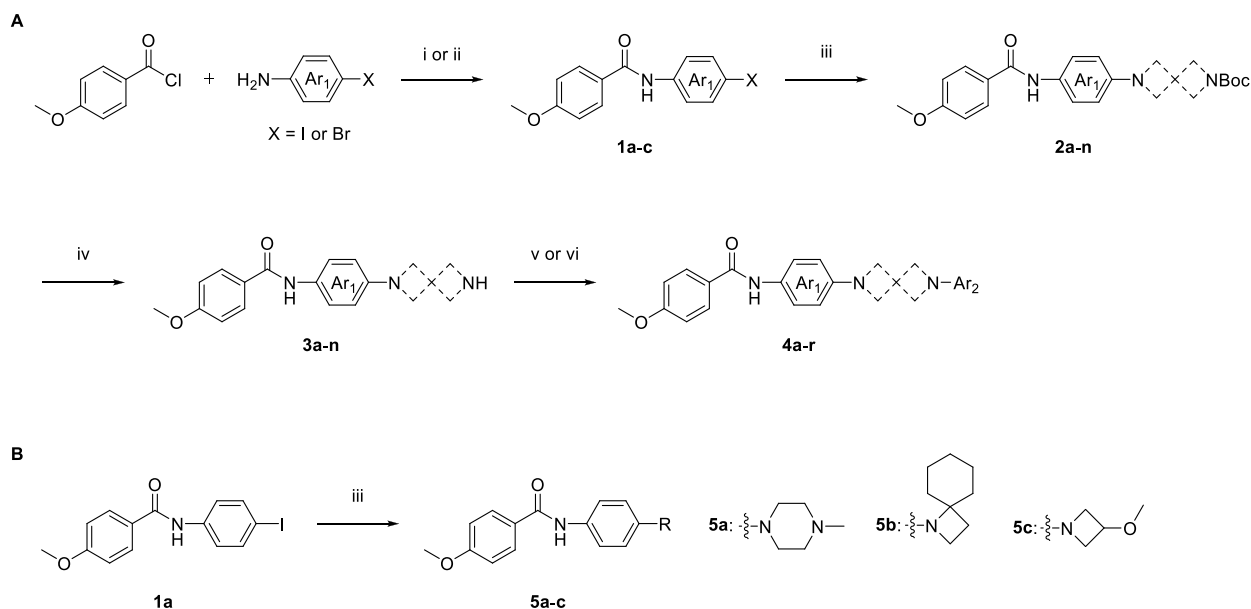
Coupling of the aromatic ring with either a diazaspirocyclic or diazabridged amine was successfully accomplished by the Pd-catalyzed Buchwald–Hartwig cross coupling reaction. The reaction proceeded in a moderate to good yield (26–88%) using a third generation (G3) Buchwald precatalyst and a mixture of NaOtBu/Cs₂CO₃ as a base.³⁷ Although the mechanism has not been fully elucidated, it is believed that Cs₂CO₃ reduces the reaction's sensitivity to moisture.

The Boc group was initially deprotected using HCl. However, even trace amounts of HCl resulted in 2,6-diazaspiro[3.3]-heptane ring-opening for compound 3a, likely due to the high strain of this spirocyclic ring system. Consequently, compounds substituted with mono- or dichloro groups were detected in ¹H NMR or LCMS data. The ring opening was avoided by instead using neat TFA, resulting in satisfactory yields (69–100%) of intermediates 3a–n.

Following deprotection to give secondary amines 3a–n, Buchwald–Hartwig cross coupling with 2-bromopyridine or 3-bromoquinoline resulted in 4a–j and 4l–r in a yield ranging from 13% to 79%. For the introduction of quinoxaline in 4k, nucleophilic aromatic substitution was performed by heating 3h with 2-bromoquinoxaline for 16 h (52% yield). Analogs 5a–c were prepared from 1a using the Buchwald–Hartwig cross coupling reaction (Scheme 1B). These analogs were designed by removing the *N*-pyridinylpiperazine moiety of BF2846 to explore the effect of Ar₂ removal from the scaffold. Yields for 5a, 5b, and 5c were 35%, 11%, and 49%, respectively.

For radiolabeling with tritium or carbon-11, the methyl on a methoxy moiety in 4-methoxy-*N*-(4-(3-(pyridin-2-yl)-3,8-diazabicyclo[3.2.1]octan-8-yl)phenyl)benzamide (4i) was removed using neat BBr₃, a strong Lewis acid (Scheme 2). The reaction proceeded for 24 h and yielded 40% of the isolated product. Since trace amounts of 4i can reduce the molar activity of radiolabeled 4i, flash chromatography was performed twice to completely purify precursor 6 from trace quantities of starting material 4i. No peak for the mass value (*m/z*) of 4i was detected in UHPLC-MS chromatograms of 6.

In Vitro Radioligand Competition Binding Assays. The target compounds were initially screened for α -syn binding affinity using recombinant α -syn fibrils by a 3-point screening assay, and the results are displayed in Figure 2 as a heatmap. The

Scheme 1. Synthesis of Heterocyclic BF2846 Analogs^a

^aReagents and conditions: (i) [for 1a or 1c] 4-methoxybenzoyl chloride, 4-iodoaniline or 6-bromopyridin-3-amine, Et₃N, CH₂Cl₂, RT, 3 h; (ii) [for 1b] 4-methoxybenzoyl chloride, 5-bromopyridine-2-amine, Et₃N, CH₂Cl₂, RT, 3 h followed by K₂CO₃, MeOH/H₂O (9:1), reflux; (iii) 1a-c, Boc-protected diazspiropamine or diazabridged amine, Pd-RuPhos-G3, RuPhos, Cs₂CO₃, NaOtBu, 1,4-dioxane, 100 °C, 3 h; (iv) TFA, RT, 20 min; (v) 3a-n, 2-bromopyridine or 3-bromoquinoline, Pd-RuPhos-G3, RuPhos, Cs₂CO₃, NaOtBu, 1,4-dioxane, 100 °C, 16 h; (vi) [for 4k] 3h, 2-bromoquinoxaline, DIPEA, DMF, 100 °C, 16 h.

three point (10 nM, 100 nM, and 1 μM) screening system has previously been used by our group in the development of other CNS radiotracers (e.g., sigma-2 receptors ligands) since it efficiently identifies potential candidates from a library of purchased or synthesized compounds.^{38,39} [³H]BF2846 was used as radioligand for the α-syn binding competition assays since it was the lead compound for the SAR study.

In the heat map, the diazspirocyclic analogs exhibited an overall low % inhibition of radioligand binding, of which the relatively larger diazspirocyclic analogs 4f and 4g showed 53% and 65% inhibition at 1 μM in the screening assay. Among diazabridged analogs, 4i having 3.8-diazabicyclo[3.2.1]octane as the amino core exhibited complete inhibition of radioligand binding at 1 μM. In contrast to 4i, bridged diamine rings containing either a one or three carbon atom bridge (i.e., 4h or 4l) displayed weak binding to α-syn. The 1,4-diazepan analog, 4m, was also tested and displayed complete inhibition of radioligand binding at 1 μM. Different heteroaromatic groups on Ar₂ were introduced within 4c, 4j, and 4k; however, the % inhibition was decreased compared to 2-pyridyl congener. Interestingly, introduction of a chlorine substituent at the para-position of the pyridine ring in Ar₂ of BF2846 dramatically decreased the binding affinity for α-syn. These data indicate that a 2-pyridine ring is the optimal substituent in Ar₂ for binding to α-syn. Lastly, replacement of the benzene ring of Ar₁ in BF2846 with a pyridine should significantly affect the physicochemical properties of BF2846 by lowering the lipophilicity of the molecule. Analogs 4o, 4p, and 4q displayed inhibition of [³H]BF2846 binding to α-syn fibrils and were advanced to the full competition assay.

Compounds with high displacement of [³H]BF2846 in the primary screening assay (i.e., ≥50% displacement of [³H]-BF2846 at 1 μM) were evaluated by generating full competition curves to determine their inhibition constants (K_i) for binding to

both recombinant α-syn fibrils and Aβ aggregates in AD brain (Table 1). The Aβ binding profile of the compounds was investigated using AD brain tissue homogenates with [³H]PiB as a radioligand. The results of the binding assays allowed for the assessment of the compound's selectivity for α-syn versus Aβ, a limitation that has hindered the development of BF2846 and its ¹⁸F-labeled analogs as an α-syn PET tracer. The full competition curves obtained for each compound are presented in Figure S1.

Table 1 shows that compounds 4i, 4m, and 4o exhibited nanomolar binding affinity for recombinant α-syn fibrils with K_i values of 6.1, 8.7, and 5.0 nM, respectively. Notably, compound 4o, which contains a piperazine moiety, demonstrated the highest α-syn affinity, but also exhibited high binding affinity for Aβ. This result is similar to that of BF2846. In contrast, compounds 4i and 4m did not exhibit any significant binding to Aβ in the [³H]PiB binding assay. Compound 4q, which was initially expected to exhibit high binding affinity for α-syn according to the heat map, showed a K_i value of only 185 nM. The K_i values of other analogs ranged from 22 to 185 nM. These heterocyclic analogs 4i and 4m exhibited selective binding to α-syn over Aβ, indicating their potential utility as PET tracers for α-synucleinopathies. In summary, based on its favorable binding affinity and selectivity, 4i was identified as a promising candidate for α-syn PET tracer.

Compound 4i was also screened for affinity for tau in radioligand binding assays using a panel of tritiated tau radioligands in post-mortem human AD, progressive supranuclear palsy (PSP), and corticobasal degeneration (CBD) tissues (Figure 3). PSP and CBD brain homogenates were chosen because they represent 4R tauopathies, where AD is a mixed 3R/4R tauopathy. The results indicate that 4i had a modest affinity to 3R/4R tau in AD tissues with a K_i value of 49 nM when [³H]MK-6240 was used as the radioligand. However, other tau radioligands were not significantly inhibited by

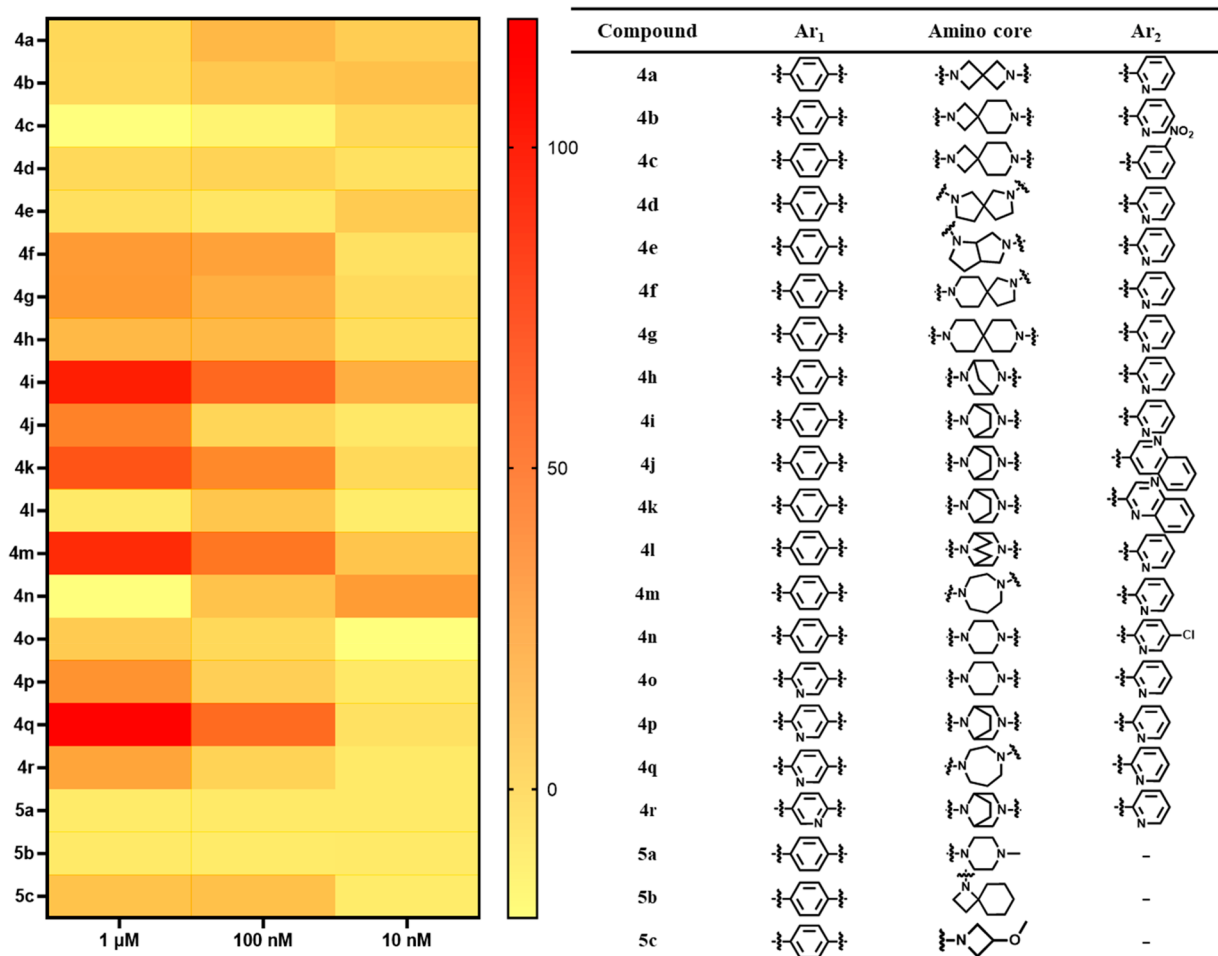
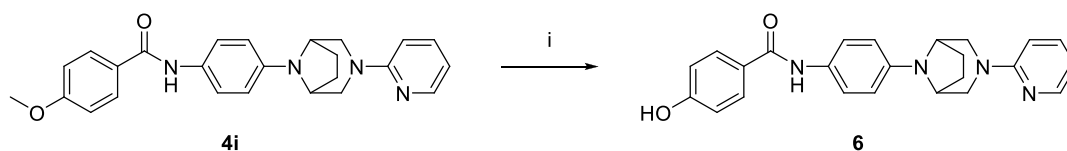


Figure 2. Heat map and structures of heterocyclic BF2846 analogs for *in vitro* α -syn binding competition assay. Extent of inhibition (%) was determined by the binding inhibition of [^3H]BF2846 (~ 4 nM) with three concentrations of tested compounds (1 μM , 100 nM, and 10 nM). Total binding or nonspecific binding was defined by the absence or the presence of 100 nM unlabeled BF2846.

Scheme 2. Synthesis of Precursor for [$^3\text{H}/^{11}\text{C}$]4i^a



^aReagents and conditions: (i) BBr_3 , CH_2Cl_2 , RT, 24 h.

unlabeled **4i**, suggesting that these radioligands and **4i** do not share the binding site in 3R/4R tau (Figure 3). Compound **4i** also had weak binding to 4R tau in PSP and CBD brain homogenates as determined by competition assays using [^3H]PM-PBB3, [^3H]CBD-2115, [^3H]PI-2620, and [^3H]AV-1451. To confirm the potential off-target binding with other G protein-coupled receptors (GPCRs) in the brain, the bindings of **4i** to a panel of GPCRs were investigated and resulted in no significant binding to these receptors (Table S1).⁴⁰

Photoaffinity Labeling Studies. To gain a better understanding of **4i** binding within α -syn fibrils, an analog (CLX**4i**) containing a diazirine cross-linking tag instead of the methoxy group was synthesized and evaluated for the binding sites (Figure 4). As we have shown previously,^{41,42} upon irradiation with light at 365 nm, CLX**4i** covalently labels α -syn, which can then be analyzed via bottom-up mass spectrometry (LC-MS/

MS) to determine the site where **4i** was bound. Photoaffinity labeling of α -syn fibrils was assessed via this workflow, and a combination of parallel digests using both trypsin and gluC enabled accurate mapping of the **4i** binding site. CLX**4i** showed cross-linking predominantly adjacent to site 9 (DMPVDPDNE, residues 115–123), along with secondary cross-links identified at site 2 (GVVHGVATVAEKTKE, residues 47–61) and in the N-terminus (EGVVAEEK, residues 15–22). These regions are folded relatively similarly in the solid state NMR structure of *in vitro* α -syn fibrils (PDB ID 2n0a) and in the cryo-EM structure of α -syn fibrils isolated from MSA patients (PDB ID 6xyo).^{30,43} Primary LC-MS/MS data are also presented in Figures S2–S4. BF2846 was previously characterized as a site 9 binder with cross-linking of an azide derivative to the 81–96 fragment of α -syn.⁴² Shifted C-terminal cross-linking suggests that **4i** binds in a

Table 1. Results of *in Vitro* Competition Binding Assay for Selected Compounds^a

compound	$K_i \pm \text{SD}$ (nM) ^b	
	α -syn	$A\beta$
4f	21.9 \pm 9.7	\geq 760
4g	>1000	N.T. ^c
4i	6.1 \pm 2.1	N.A. ^d
4j	108 \pm 33	>1000
4k	47.6 \pm 14.0	N.T.
4m	8.7 \pm 0.6	>1000
4o	4.9 \pm 0.4	43.1 \pm 3.8
4p	44.1 \pm 32.0	N.A.
4q	185 \pm 120	N.A.

^a K_i values were determined from competitive radioligand binding full curves using recombinant α -syn fibrils with [³H]BF2846 and AD (CAA-) homogenates with [³H]PiB. ^bThe K_i values are expressed as the mean \pm SD of three individual experiments. ^cN.T.: not tested. ^dN.A.: not active (no displacement at 1000 nM).

Radioligand	Tissue	K_i (nM)
[³ H]MK-6240	AD	49
[³ H]JPM-PBB3	AD	140
[³ H]JPM-PBB3	PSP	180
[³ H]JPM-PBB3	CBD	540

Radioligand	Tissue	K_i (nM)
[³ H]PI-2620	AD	>1000
[³ H]PI-2620	PSP	>1000
[³ H]PI-2620	CBD	830

Radioligand	Tissue	K_i (nM)
[³ H]AV-1451	AD	>1000
[³ H]AV-1451	PSP	>1000
[³ H]AV-1451	CBD	>1000

Figure 3. Competition binding of 4i vs different tritiated tau radioligands in AD, PSP, and CBD tissues. All assays were performed in triplicate.

slightly different orientation than BF2846, although this may partially be attributed to the longer diazirine cross-linking tag.

***In Vitro* Saturation Binding Assays.** Due to the potential differences between α -syn fibrils and patient brain-derived α -syn aggregates,⁴³ it is necessary to determine the maximum binding capacity (B_{max}) and the dissociation constant (K_D) of [³H]4i in both PD and MSA brain homogenates as well as α -syn fibrils (Figure 5). In addition, saturation binding of [³H]4i for K_D measurements was assessed in AD, PSP, and CBD brain homogenates (Figure S5). The comprehensive data set is summarized in Table 2.

Consistent with inhibition assays, it was found that [³H]4i had a high binding affinity to α -syn fibrils and the synucleinopathies PD and MSA. It is of interest to note that the K_D values of [³H]4i to α -syn fibrils was similar to that observed in the synucleinopathies PD and MSA. Contrary to what was expected from the data shown in Figure 3, [³H]4i exhibited high binding in AD homogenates and in PSP and CBD homogenates. Since the PSP and CBD samples used in the binding assay were devoid of $A\beta$ and α -syn, the binding of [³H]4i likely reflects binding to 4R tau. Detailed *in vitro* autoradiography studies demonstrating the colocalization of [³H]4i binding with tau and not $A\beta$ in tissue sections of AD, PSP, and CBD brain will be published separately. However, the *in vitro* binding data described above (Table 2) suggest that [³H]4i binds with high affinity to aggregated tau proteins, in particular 3R/4R tau in AD and 4R tau in PSP and CBD.

CLX4i

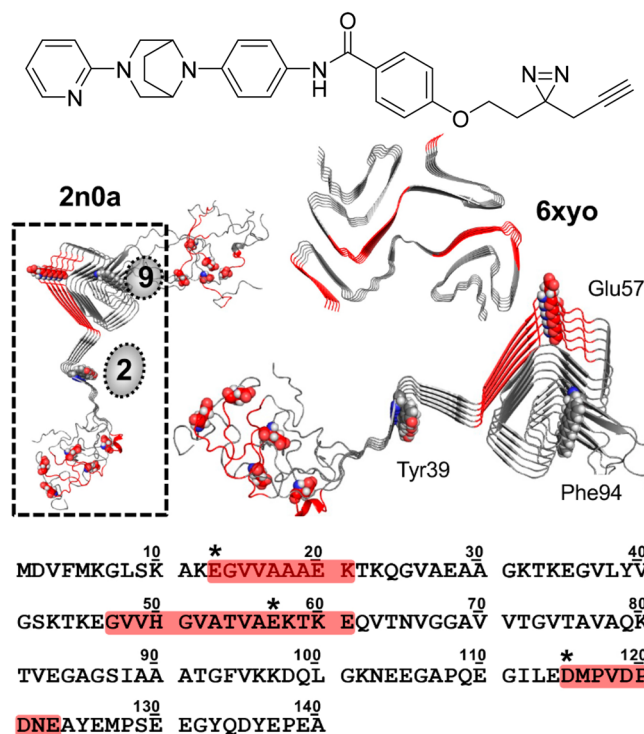


Figure 4. Structure of photoreactive ligand CLX4i and putative binding sites of α -syn fibril cross-linking. Cross-linked peptides from trypsin and GluC digests are highlighted in red on the sequence and on the 2n0a (full structure and zoom-in of boxed region) or 6xyo fibril structures. Sites 2 and 9 are indicated within the 2n0a structure. Cross-linked residues indicated with * in the sequence and shown as spheres in the structure. Tyr39 and Phe94 are also represented as spheres.

Autoradiography. Nuclear emulsion autoradiography of [³H]4i was performed on PD and MSA tissues to assess its binding affinity with α -syn aggregates known to exhibit structural variations (Figure 6). Nuclear emulsion autoradiography is a highly sensitive technique for detecting and visualizing the presence of radioactive material in a sample, offering excellent spatial resolution down to a few micrometers. The images revealed that [³H]4i more clearly identified α -syn aggregates in MSA compared to PD. The findings of this study suggest that [³H]4i may have a strong binding affinity with GCIs rather than LBs. The localization of α -syn aggregates in PD and MSA was confirmed by α -syn antibody using fluorescence microscopy.

To confirm the results observed in the nuclear emulsion autoradiography study, autoradiography studies were also conducted in tissue sections in PD (hippocampus), MSA (cerebellum), and age-matched control (frontal cortex) brain samples. The tissue sections for PD brain had high levels of α -syn and $A\beta$, whereas the MSA brain sections had only α -syn in the form of GCIs. The control brain was negative for α -syn and $A\beta$. The results of this study (Figure 7) clearly show that [³H]4i binds to α -syn in MSA and not PD and control brain sections. The low binding of [³H]4i in the region that contains $A\beta$ plaques is also consistent with the *in vitro* binding assays, suggesting that this radioligand binds with weak affinity to $A\beta$ plaques. Blocking studies with unlabeled 4i confirm that the binding of [³H]4i is displaceable in MSA brain (Figure S6).

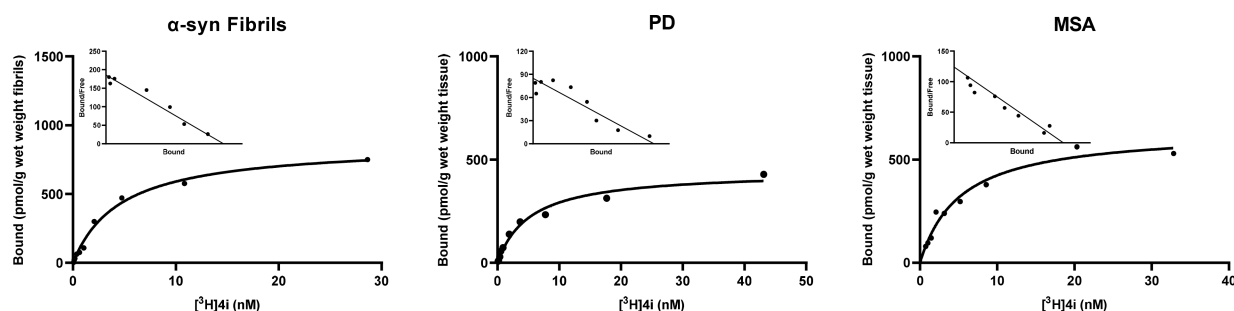


Figure 5. Representative saturation binding curves of [^3H]4i in α -syn fibrils and brain tissue homogenates derived from patients with PD or MSA. The curves were drawn based on the specific binding of [^3H]4i, which was determined by subtracting the nonspecific binding from the total binding. Total binding or nonspecific binding was defined by the absence or the presence of 100 nM unlabeled BF2846.

Table 2. Summary of Saturation Binding Assays for Various Neurodegenerative Diseases

	[^3H]4i					
	synthetic fibrils	PD	MSA	AD	PSP	CBD
K_D (nM) ^a	3.0 \pm 1.4	5.0 \pm 1.6	7.1 \pm 2.3	5.9 \pm 0.6	7.0 \pm 3.0	18 \pm 7.5
B_{max} (nM)	690 \pm 237	457 \pm 184	773 \pm 144	1209 \pm 391	280 \pm 120	540 \pm 230

^aThe K_D values are expressed as the mean \pm SD of three individual experiments.

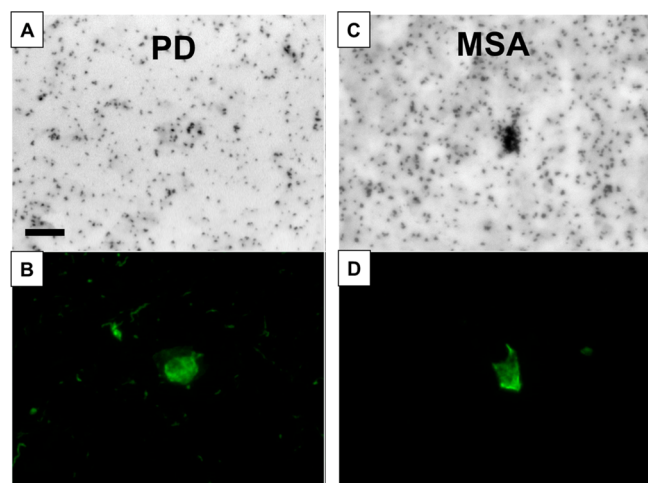


Figure 6. Images of nuclear emulsion autoradiography for the binding affinity of [^3H]4i with α -syn aggregates in PD (A) and MSA tissues (C). Fluorescence immunostaining with α -syn antibody was also performed on the same PD and MSA sections to identify α -syn aggregates in LBs (B) and GCIs (D), respectively ($n = 1$). The scale bar represents 10 μm .

The autoradiography data described above are not in agreement with the radioligand binding studies in brain tissue homogenates (Table 2). The autoradiography data suggest that the binding affinity of [^3H]4i in PD tissue sections is not as high as the *in vitro* binding assays conducted in PD brain homogenates. The reasons for this discrepancy are not clear, but our results highlight the need to confirm data obtained in radioligand binding assays using tissue homogenates with autoradiography studies in tissue sections of post-mortem brain samples. We are currently conducting more detailed studies with [^3H]4i to identify factors that may be responsible for this discrepancy between homogenate binding assays and autoradiography in tissue sections.

Radiosynthesis. To enable *in vivo* imaging of α -syn in the brain, we employed a typical $\text{S}_{\text{N}}2$ reaction using gas-phase carbon-11 in an automated synthesis module for [^{11}C]4i (Scheme 3). The hydroxyl precursor **6**, obtained by removal

of a methoxy moiety from **4i**, was used for the synthesis of [^{11}C]4i. The crude product for [^{11}C]4i was purified using preparative HPLC (Figure S7) and subsequently formulated for injection. Total synthesis time was 40 min, and the radiochemical yield (RCY) was 8.0 \pm 2.9% (decay corrected to end of bombardment), yielding 1079 \pm 404 MBq of isolated activity ($n = 4$). The radiochemical purity and the molar activity for prepared [^{11}C]4i were determined by analytical HPLC (Figure S8) and found to be over 99% and 106 \pm 56 GBq/ μmol , respectively. These results demonstrate that the radiosynthesis of [^{11}C]4i is suitable for further preclinical and clinical studies.

Predicting Blood–Brain Barrier (BBB) Penetration. The development of CNS imaging PET tracers faces several challenges, with BBB penetration being one of the most significant. To predict BBB penetration of heterocyclic analogs including **4i**, the Brain Or Intestinal Estimated permeation method (BOILED-Egg) was performed^{44,45} (Figure S9). This method was proposed for the brain access of small molecules based on the partition coefficient that was developed by Wildman and Crippen (WLOGP)⁴⁶ and the topological polar surface area (tPSA). In the BOILED-Egg plot, **4i** was placed in the yolk, suggesting this compound is BBB-penetrant. In order to improve the accuracy of the prediction, $\text{LogD}_{7.4}$ of [^{11}C]4i was experimentally confirmed using the shake-flask method, resulting in a value of 2.52 \pm 0.01 ($n = 5$). Thus, [^{11}C]4i possesses suitable physicochemical properties for *in vivo* brain PET imaging studies.

In Vivo Brain PET Analysis of [^{11}C]4i in Nonhuman Primates (NHPs). A dynamic PET study was carried out in NHPs to investigate the potential of [^{11}C]4i as an *in vivo* brain PET tracer, with a focus on pharmacokinetic and imaging properties (Figure 8). As predicted by BOILED-Egg plot modeling based on favorable physicochemical properties, [^{11}C]4i showed BBB penetration in the initial PET images. The PET images demonstrated that [^{11}C]4i exhibited relatively high uptake in the putamen and cerebellum, particularly. The time-activity curves (TACs) revealed that the peak uptake of the whole brain occurred at 4 min with standardized uptake value (SUV) of 1.68 \pm 0.54. Furthermore, the brain concentration of [^{11}C]4i decreased rapidly over time, with no significant signals

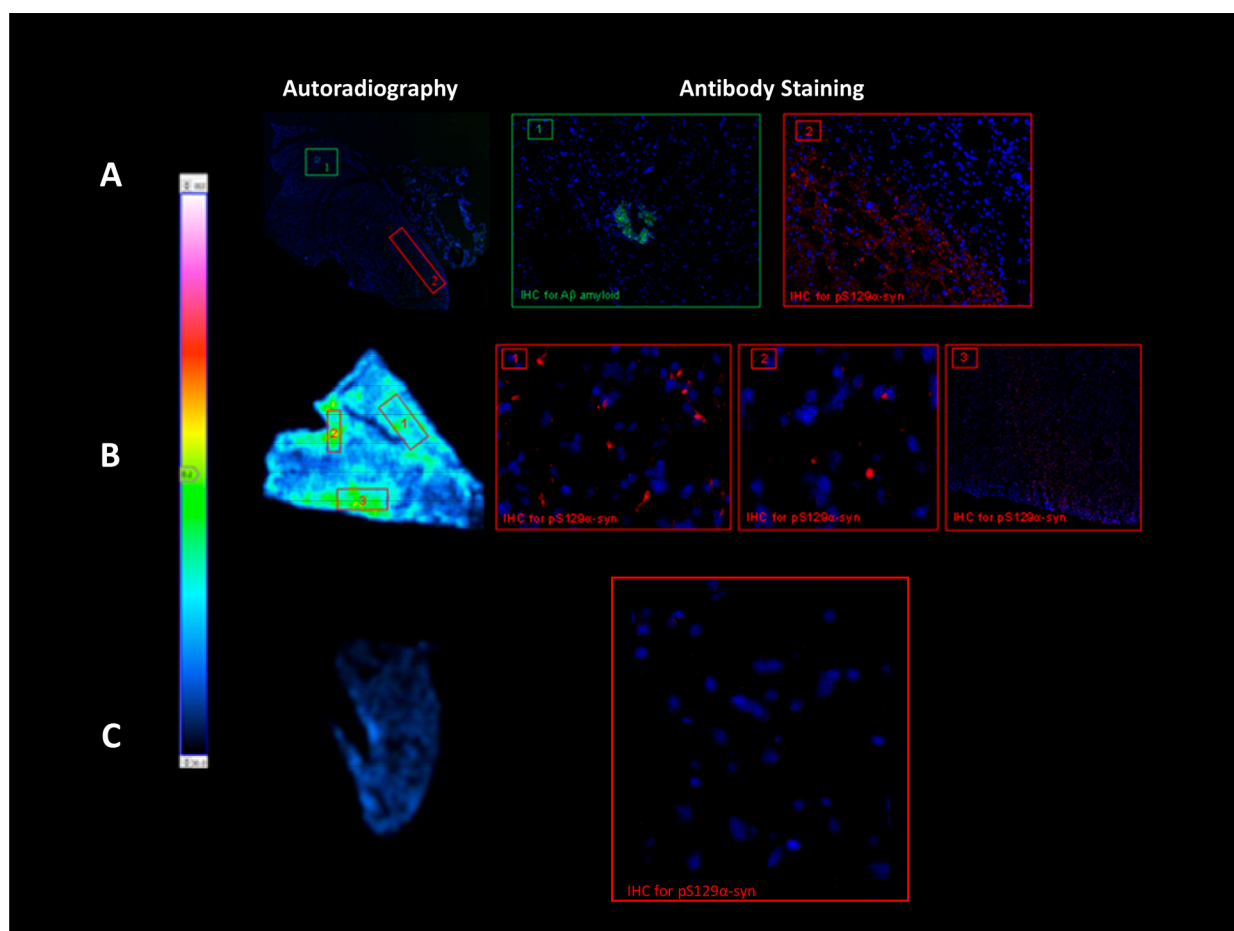
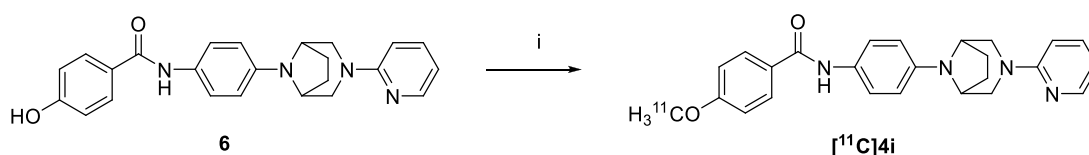


Figure 7. *In vitro* autoradiography data in PD (A), MSA (B), and control (C) tissue sections. There was low binding of [^3H]4i in PD and control brain, whereas high binding was observed in MSA ($n = 1$).

Scheme 3. Radiosynthesis of [^{11}C]4i^a



^aReagents and conditions: (i) [^{11}C]MeI, 5 N NaOH, DMF, 70 °C, 5 min.

observed at 30–40 min after injection ($\text{SUV} = 0.85 \pm 0.18$). The brain concentration ratio between 4 and 60 min was approximately 2.5, indicating [^{11}C]4i should have a high signal-to-background ratio for imaging α -syn aggregates. Therefore, the demonstrated good brain permeability and rapid washout suggest that [^{11}C]4i is a suitable candidate for an *in vivo* brain PET tracer. Whole body distribution PET images and TACs are presented in Figure S10.

Metabolism Study. Since radiometabolites can influence a tracer's efficacy as PET imaging agent, metabolite profiling was performed by HPLC analysis of NHP blood. The obtained chromatograms demonstrated that [^{11}C]4i underwent metabolism, yielding one major polar metabolite along with minor metabolites within 30 min. The percentage of the parent [^{11}C]4i remaining at 5, 15, and 30 min amounted to 58%, 28%, and 14%, respectively. Under the same condition, an additional HPLC chromatogram was examined to identify potential metabolites. The predominantly polar metabolite observed in the assay

corresponded to the retention time of 4-methoxybenzamide, while a minor metabolite, *N*-(4-(3,8-diazabicyclo[3.2.1]octan-8-yl)phenyl)-4-[^{11}C]methoxybenzamide, was also detected. *In vitro* assays were conducted to assess the binding affinity of potential metabolites, such as *N*-(4-(3,8-diazabicyclo[3.2.1]octan-8-yl)phenyl)-4-methoxybenzamide and 4-methoxy-*N*-phenylbenzamide, for α -syn *in vitro*. In the assay, these compounds exhibited no binding to recombinant α -syn. Although the BOILED-Egg modeling predicted BBB penetrance for these metabolites, the polar metabolites are likely to be cleared from the brain, as shown in the brain PET images.

DISCUSSION

In vivo imaging of α -syn has significant implications for the early diagnosis, monitoring, and the assessment of therapeutic intervention of the family of neurodegenerative disorders referred to as the synucleinopathies. Since the current diagnosis of α -synucleinopathies based on clinical symptoms and

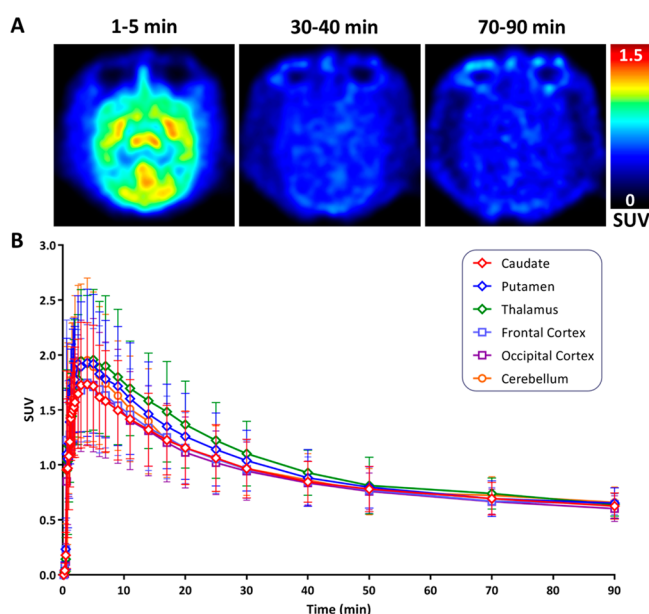


Figure 8. *In vivo* brain PET study of [^{11}C]4i in NHP. Dynamic PET images were obtained for 90 min, and representative examples are presented by summing images acquired during 1–5, 30–40, and 70–90 min (A). TACs were obtained by quantification of uptake of [^{11}C]4i in different brain regions (B) ($n = 3$).

neuroimaging techniques such as MRI is limited in detecting α -syn pathology in the early stages of the disease,⁴⁷ numerous studies have focused on developing ligands with high binding affinity that can specifically localize α -syn.^{27,41,48,49} The necessary criteria for *in vivo* CNS imaging studies as a PET tracer include high binding affinity and selectivity for the target of interest and good physicochemical properties leading to high initial brain uptake and fast washout from regions representing nonspecific binding of the radiotracer.

The objective of this study was to conduct an SAR study investigating the replacement of the piperazine moiety of the lead compound, BF2846, with bridged or spirocyclic diamines. We previously demonstrated that this substitution was successful in developing selective ligands for other protein targets, including the dopamine D3 receptor,³⁶ sigma-2 receptor,³⁹ or PARP-1.⁵⁰ We hypothesized that this isosteric replacement of the piperazine ring may improve the selectivity of this scaffold for α -syn versus $A\beta$ fibrils. Our efforts focused on BF2846 since we have shown that it preferentially binds to site 9 (G86-F94-K96) within α -syn fibrils,³⁵ which is expected to be less influenced by posttranslational modification of α -syn compared to other binding sites.⁵¹ It is noteworthy that phosphorylation at S129 accounts for up to 90% of α -syn in LBs and phosphorylated S87 or Y39 has also been observed in post-mortem brain tissues from PD or MSA patients.^{52–54}

The results from *in vitro* binding assays showed that 4i containing the 3.8-diazabicyclo[3.2.1]octane moiety exhibited a nanomolar binding affinity for α -syn and had a lower binding affinity for $A\beta$ presented in tissue homogenates from AD brain. Although the mechanism behind this selectivity is not well understood, it is possible that the geometric difference between 4i and BF2846 could be responsible⁵⁵ for this observation. We also found that 4i binds somewhat differently to *in vitro* α -syn fibrils than BF2846 based on cross-linking studies, which could also be due to the geometric differences between 4i and BF2846. It is of interest to note that the sites to which 4i binds are

relatively well-conserved between *in vitro* fibrils (2n0a) and fibrils isolated from MSA patients (6xyo, Figure 4). This observation supports the favorable binding to MSA tissue observed in the autoradiography studies.

Although replacement of the piperazine moiety of BF2846 with the 3.8-diazabicyclo[3.2.1]octane moiety in 4i increased the selectivity for α -syn versus $A\beta$, [^3H]4i displayed high binding affinity for AD, CBD, and PSP tissue homogenates, indicating high affinity binding of [^3H]4i to aggregated tau. Interestingly, this result may reflect binding to a novel site on aggregated tau since 4i did not have high affinity for displacing the known tau radioligands [^3H]PM-PBB3, [^3H]CBD-2115, [^3H]PI-2620, and [^3H]AV-1451 in homogenate assays. PET imaging studies in NHPs also indicated that [^{11}C]4i had good brain uptake and rapid tracer washout from the brain, thereby increasing the potential for successful *in vivo* imaging of MSA with PET. In the metabolism study, [^{11}C]4i was rapidly metabolized into polar metabolites. Notably, these metabolites showed no binding to α -syn fibrils. [^{11}C]4i is in the process of being advanced to first-in-human imaging studies in control subjects and MSA patients.

CONCLUSION

The goal of this study was to develop a PET tracer for α -syn detection in the brain by conducting an SAR investigation on BF2846. Our SAR study led to the identification of a promising candidate, 4i, and *in vitro* binding assays demonstrated its high affinity and selectivity for α -syn versus $A\beta$ aggregates. Moreover, the ability to detect α -syn aggregates in MSA but not PD was demonstrated by nuclear emulsion and autoradiography in tissue sections. These data suggest that [^{11}C]4i may be more useful in detecting GCIs in patients with MSA than LBs in patients with PD. The high binding affinity for tau proteins may limit the utility of [^{11}C]4i under certain circumstances. However, the absence of tau in the cerebellum suggests that it may be possible to image α -syn GCIs in MSA-Cerebellar type subjects. The favorable pharmacokinetic properties of [^{11}C]4i for *in vivo* brain imaging observed in our study, including high binding affinity for α -syn, high initial brain uptake, and rapid washout, suggest that this PET tracer may be useful for early detection and monitoring of MSA.

EXPERIMENTAL SECTION

General. Commercial reagents and solvents were purchased from reputable sources, including Sigma-Aldrich (MO, U.S.A.), Synthonix (NC, U.S.A.), Enamine (Kyiv, UA), or Thermo Fisher Scientific (MA, U.S.A.), and used as received. Compounds 1a–c were synthesized by the modification of known literature.³⁴ Thin layer chromatography (TLC) was performed using TLC silica gel 60W F254S plates for monitoring reactions, and the spots were visualized under UV light (254 nm). Flash chromatography purifications were conducted on a Biotage Isolera One system (Uppsala, Sweden). ^1H and ^{13}C NMR spectra were recorded on a Bruker NEO-400 spectrometer (Bruker, MA, U.S.A.) with chemical shifts (δ) reported in parts per million (ppm) relative to the deuterated solvent as an internal reference. Mass spectra (m/z) were acquired on a 2695 Alliance LC-MS (Waters Corporation, MA, U.S.A.) with positive electrospray ionization (ESI⁺), and high resolution mass spectra (HRMS, m/z) were obtained using a waters LCT premier mass spectrometer (Waters Corporation, MA, U.S.A.). The purity of investigated analogs was determined prior to the screening and confirmed to be >95% by UHPLC-MS (Table S3). Recombinant α -syn fibrils preparation including α -syn protein expression and purification was performed according to the literature.¹⁰ For $A\beta$ assay, AD brain sample was provided by the Penn Brain Bank, and most of the white matter was removed before weighing the tissue. AD brain homogenates were prepared and stored at $-80\text{ }^\circ\text{C}$ before each

binding assay.⁵⁶ Human PD tissue sample used in the homogenate binding assays was provided by Dr. Thomas Beach of the Banner Sun Health Research Institute, Sun City, AZ. Experiments with human post-mortem tissues were approved by the institutional review board and performed in accordance with the 1964 Declaration of Helsinki. All animal studies were performed under protocols approved by the University of Pennsylvania Institutional Animal Care and Use Committee. The University of Pennsylvania is AAALAC accredited, and its PHS Office of Animal Welfare Assurance Number is D16-00045 (A3079-01).

General Methods. General Procedure A: Buchwald–Hartwig Cross Coupling for the Synthesis of 2a–q. To a solution of 1a–c (1 equiv) and Boc-protected spirocyclic or bridged diamines (1.1 equiv) in 1,4-dioxane (0.15 M), Pd-RuPhos-G3 (0.01 equiv), RuPhos (0.02 equiv), Cs₂CO₃ (1 equiv), and NaOtBu (3 equiv) were added. The mixture was sonicated for 1 min and heated at 100 °C for 3 h. After cooling to RT, the mixture was diluted with ethyl acetate and washed using water and brine, dried over Na₂SO₄, and filtered. The volatiles were removed under reduced pressure, and the crude product was purified by flash chromatography on silica gel (0% to 80% EtOAc/*n*-Hexane with gradient elution).

General Procedure B: Boc Deprotection for the Synthesis of 3a–n. To a vial of 2a–n (1 equiv), TFA (60 equiv) was added. The mixture was stirred for 20 min, and the volatiles were removed under reduced pressure. Five mL of 7 N NH₃ in MeOH was added, and the volatiles were removed under pressure. The residue was diluted with CH₂Cl₂ and washed using aq saturated NaHCO₃ solution with NaOH (pH 9–10). The inorganic layer was extracted by CH₂Cl₂, and the combined organic layer was collected, dried over Na₂SO₄, filtered, and concentrated *in vacuo*. The crude product was purified by flash chromatography on silica gel (CH₂Cl₂/7 N NH₃ in MeOH = 15:1).

General Procedure C: Buchwald–Hartwig Cross Coupling for the Synthesis of 4a–r. To a solution of 3a–n (1 equiv) and 2-bromopyridine or 3-bromoquinoline (2 equiv) in 1,4-dioxane (0.15 M), Pd-RuPhos-G3 (0.01 equiv), RuPhos (0.02 equiv), Cs₂CO₃ (1 equiv), and NaOtBu (3 equiv) were added. The mixture was sonicated for 1 min and heated at 100 °C for 16 h. After cooling to RT, the mixture was diluted with ethyl acetate and washed using water and brine, dried over Na₂SO₄, and filtered. The volatiles were removed under reduced pressure, and the crude product was purified by flash chromatography on silica gel (0% to 50% EtOAc/*n*-Hexane with gradient elution and CH₂Cl₂/7 N NH₃ in MeOH = 40:1).

***N*-(4-Iodophenyl)-4-methoxybenzamide (1a).** To a solution of 4-methoxybenzoyl chloride (4.1 mL, 30.1 mmol) in 91 mL of CH₂Cl₂, 4-iodoaniline (6 g, 27.4 mmol) and Et₃N (3.8 mL, 27.4 mmol) were slowly added. The reaction mixture was stirred for 3 h at RT. After the reaction was completed, the mixture was filtered and the filtrate was washed with diethyl ether for 2–3 times. The filtrate was dried *in vacuo*, and 1a (9 g, 93% yield) was obtained as a white solid. (¹H NMR, 400 MHz, DMSO-*d*₆): δ = 10.17 (s, 1H), 7.95 (dt, *J*₁ = 8.9 Hz, *J*₂ = 2.8 Hz, 2H), 7.68 (dt, *J*₁ = 8.9 Hz, *J*₂ = 2.2 Hz, 2H), 7.63 (dt, *J*₁ = 9.0 Hz, *J*₂ = 2.2 Hz, 2H), 7.07 (dt, *J*₁ = 8.9 Hz, *J*₂ = 2.9 Hz, 2H), 3.84 (s, 3H); (¹³C NMR, 100 MHz, DMSO-*d*₆): δ = 164.9, 162.0, 139.2, 137.2, 129.6, 126.7, 122.4, 113.6, 86.9, 55.4; ESI-MS *m/z* calculated for C₁₄H₁₃INO₂⁺ [M + H]⁺ 354.2; found 354.0.

***N*-(5-Bromopyridin-2-yl)-4-methoxybenzamide (1b).** The intermediate having two 4-methoxybenzamide was synthesized in the same procedure as 1a, and 3.6 g (41%) was obtained as a white solid. The eluent was removed under reduced pressure, and the residue was dissolved in MeOH and a water mixture (100 mL, 9:1). After adding K₂CO₃ (1 g, 7.7 mmol), the mixture was refluxed for 13 min. After completion of the reaction, the mixture was diluted with CH₂Cl₂, washed with water, dried over MgSO₄, filtered, and concentrated *in vacuo*. The crude product was purified by flash chromatography on silica gel (0% to 100% EtOAc/*n*-Hexane with gradient elution) to afford 1b (2.4 g, 38% yield for 2 steps) as a white solid. (¹H NMR, 400 MHz, DMSO-*d*₆): δ = 10.80 (s, 1H), 8.50 (d, *J* = 2.2 Hz, 1H), 8.18 (d, *J* = 8.9 Hz, 1H), 8.06–8.02 (m, 3H), 7.04 (dt, *J*₁ = 8.9 Hz, *J*₂ = 2.9 Hz, 2H), 3.84 (s, 3H); (¹³C NMR, 100 MHz, DMSO-*d*₆): δ = 165.4, 162.3,

151.4, 148.4, 140.5, 130.1, 125.8, 116.2, 113.7, 113.6, 55.4; ESI-MS *m/z* calculated for C₁₃H₁₁BrN₂O₂⁺ [M]⁺ 307.1; found 307.2.

***N*-(6-Bromopyridin-3-yl)-4-methoxybenzamide (1c).** 1c was synthesized in the same procedure as 1a and obtained 450 mg (25% yield) as a white solid. (¹H NMR, 400 MHz, DMSO-*d*₆): δ = 10.41 (s, 1H), 8.79 (d, *J* = 2.7 Hz, 1H), 8.16 (dd, *J*₁ = 8.7 Hz, *J*₂ = 2.8 Hz, 1H), 7.98 (d, *J* = 8.7 Hz, 2H), 7.63 (d, *J* = 8.6 Hz, 1H), 7.09 (d, *J* = 8.8 Hz, 2H), 3.85 (s, 3H); (¹³C NMR, 100 MHz, DMSO-*d*₆): δ = 165.2, 162.3, 142.0, 136.0, 134.1, 130.6, 129.8, 127.7, 126.0, 113.7, 55.5; ESI-MS *m/z* calculated for C₁₃H₁₁BrN₂O₂⁺ [M]⁺ 307.1; found 307.2.

***tert*-Butyl 6-(4-(4-Methoxybenzamido)phenyl)-2,6-diazaspiro[3.3]heptane-2-carboxylate (2a).** 2a was synthesized using 1a (353 mg, 1 mmol) and *tert*-butyl 2,6-diazaspiro[3.3]heptane-2-carboxylate (243 mg, 1 mmol) in general procedure A to afford 2a (365 mg, 86% yield) as a white solid. (¹H NMR, 400 MHz, DMSO-*d*₆): δ = 9.82 (s, 1H), 7.92 (d, *J* = 8.8 Hz, 2H), 7.53 (d, *J* = 8.8 Hz, 2H), 7.03 (d, *J* = 8.8 Hz, 2H), 6.41 (d, *J* = 8.8 Hz, 2H), 4.02 (s, 4H), 3.89 (s, 4H), 3.83 (s, 3H), 1.38 (s, 9H); (¹³C NMR, 100 MHz, DMSO-*d*₆): δ = 164.2, 161.6, 155.3, 148.0, 129.9, 129.3, 127.2, 121.8, 113.5, 111.5, 78.6, 61.8, 55.3, 32.9, 28.0; ESI-MS *m/z* calculated for C₂₄H₃₁N₃O₄⁺ [M + 2H]⁺ 425.5; found 425.5.

***tert*-Butyl 2-(4-(4-Methoxybenzamido)phenyl)-2,7-diazaspiro[3.5]nonane-7-carboxylate (2b).** 2b was synthesized using 1a (353 mg, 1 mmol) and *tert*-butyl 2,7-diazaspiro[3.5]nonane-7-carboxylate (263 mg, 1 mmol) in general procedure A to afford 2b (340 mg, 75% yield) as a white solid. (¹H NMR, 400 MHz, DMSO-*d*₆): δ = 9.81 (s, 1H), 7.93 (d, *J* = 8.8 Hz, 2H), 7.53 (d, *J* = 8.8 Hz, 2H), 7.04 (d, *J* = 8.9 Hz, 2H), 6.41 (d, *J* = 8.8 Hz, 2H), 3.83 (s, 3H), 3.55 (s, 4H), 3.32 (t, *J* = 6.6 Hz, 4H+water), 1.69 (t, *J* = 5.5 Hz, 4H), 1.41 (s, 9H); (¹³C NMR, 100 MHz, DMSO-*d*₆): δ = 164.2, 161.6, 153.9, 148.3, 129.4, 129.3, 127.2, 121.9, 113.5, 111.0, 78.6, 61.4, 55.3, 35.1, 34.2, 28.1; ESI-MS *m/z* calculated for C₂₆H₃₃N₃O₄⁺ [M + H]⁺ 452.6; found 452.6.

***tert*-Butyl 7-(4-(4-Methoxybenzamido)phenyl)-2,7-diazaspiro[4.4]nonane-2-carboxylate (2c).** 2c was synthesized using 1a (170 mg, 0.48 mmol) and *tert*-butyl 2,7-diazaspiro[4.4]nonane-2-carboxylate (120 mg, 0.53 mmol) in general procedure A to afford 2c (70 mg, 32% yield) as a yellow oil. (¹H NMR, 400 MHz, CD₃CN): δ = 8.40 (s, 1H), 7.88 (dt, *J*₁ = 8.9 Hz, *J*₂ = 2.9 Hz, 2H), 7.46 (d, *J* = 8.9 Hz, 2H), 7.01 (dt, *J*₁ = 8.9 Hz, *J*₂ = 2.9 Hz, 2H), 6.55 (d, *J* = 9.0 Hz, 2H), 3.84 (s, 3H), 3.41–3.35 (m, 4H), 3.29–3.22 (m, 4H), 2.04–1.97 (m, 2H), 1.92–1.85 (m, 2H), 1.44 (d, *J* = 5.3 Hz, 9H); (¹³C NMR, 100 MHz, CD₃CN): δ = 165.3, 162.7, 154.9, 145.9, 129.6, 128.4, 128.2, 123.2, 114.2, 112.0, 79.0, 57.5, 55.8, 47.6, 45.7, 45.4, 35.7, 35.1, 28.3; ESI-MS *m/z* calculated for C₂₆H₃₃N₃O₄⁺ [M + H]⁺ 452.6; found 452.6.

***tert*-Butyl 1-(4-(4-Methoxybenzamido)phenyl)hexahydropyrrolo[3,4-*b*]pyrrole-5(1H)-carboxylate (2d).** 2d was synthesized using 1a (353 mg, 1 mmol) and *tert*-butyl hexahydropyrrolo[3,4-*b*]pyrrole-5(1H)-carboxylate (212 mg, 1 mmol) in general procedure A to afford 2d (272 mg, 62% yield) as a green waxy solid. (¹H NMR, 400 MHz, MeOD): δ = 7.89 (d, *J* = 8.8 Hz, 2H), 7.47 (d, *J* = 8.8 Hz, 2H), 6.97 (d, *J* = 8.8 Hz, 2H), 6.50 (d, *J* = 8.8 Hz, 2H), 4.09 (brs, 1H), 3.82 (s, 3H), 3.59 (dd, *J*₁ = 11.6 Hz, *J*₂ = 6.2 Hz, 1H), 3.50 (q, *J* = 7.0 Hz, 2H), 3.38–3.35 (m, 1H + MeOH), 3.30 (dd, *J*₁ = 11.3 Hz, *J*₂ = 4.7 Hz, 1H), 3.22 (q, *J* = 7.4 Hz, 1H), 2.14–2.06 (m, 1H), 1.86–1.79 (m, 1H), 1.43 (d, *J* = 10.2 Hz, 9H); (¹³C NMR, 100 MHz, MeOD): δ = 168.0, 163.9, 156.5, 145.7, 130.5, 129.3, 128.4, 124.4, 114.8, 113.5, 81.1, 56.1, 50.0, 30.5, 28.9; ESI-MS *m/z* calculated for C₂₅H₃₂N₃O₄⁺ [M + H]⁺ 438.5; found 438.6.

***tert*-Butyl 8-(4-(4-Methoxybenzamido)phenyl)-2,8-diazaspiro[4.5]decane-2-carboxylate (2e).** 2e was synthesized using 1a (200 mg, 0.56 mmol) and *tert*-butyl 2,8-diazaspiro[4.5]decane-2-carboxylate (150 mg, 0.62 mmol) in general procedure A to afford 2e (80 mg, 31% yield) as a white solid. (¹H NMR, 400 MHz, Acetone-*d*₆): δ = 9.21 (s, 1H), 7.97 (dt, *J*₁ = 8.8 Hz, *J*₂ = 3.6 Hz, 2H), 7.67 (d, *J* = 9.0 Hz, 2H), 7.02 (d, *J* = 8.8 Hz, 2H), 6.96 (d, *J* = 9.0 Hz, 2H), 3.87 (s, 3H), 3.38 (q, *J* = 7.4 Hz, 2H), 3.21 (d, *J* = 6.2 Hz, 4H), 3.15–3.08 (m, 2H), 1.80 (q, *J* = 7.2 Hz, 2H), 1.70 (t, *J* = 5.4 Hz, 4H), 1.44 (s, 9H); (¹³C NMR, 100 MHz, Acetone-*d*₆): δ = 166.1, 164.0, 150.1, 139.3, 133.5, 131.2, 130.9, 129.6, 123.9, 123.0, 118.3, 115.4, 115.3, 56.7, 49.0, 48.9, 36.2, 29.6, 0.9;

ESI-MS m/z calculated for $C_{27}H_{37}N_3O_4^+$ $[M + 2H]^+$ 467.6; found 467.6.

tert-Butyl 9-(4-(4-Methoxybenzamido)phenyl)-3,9-diazaspiro[5.5]undecane-3-carboxylate (2f). 2f was synthesized using 1a (353 mg, 1 mmol) and *tert*-butyl 3,9-diazaspiro[5.5]undecane-3-carboxylate (254 mg, 1 mmol) in general procedure A to afford 2f (185 mg, 39% yield) as a white solid. (1H NMR, 400 MHz, MeOD): δ = 7.90 (dt, J_1 = 8.8 Hz, J_2 = 2.8 Hz, 2H), 7.52 (d, J = 9.0 Hz, 2H), 7.01 (td, J_1 = 7.3 Hz, J_2 = 2.0 Hz, 4H), 3.87 (s, 3H), 3.44 (t, J = 5.0 Hz, 4H), 3.16 (t, J = 5.6 Hz, 4H), 1.69 (t, J = 5.7 Hz, 4H), 1.50 (t, J = 5.8 Hz, 4H), 1.46 (s, 9H); (^{13}C NMR, 100 MHz, DMSO- d_6): δ = 164.2, 161.6, 153.9, 147.6, 130.7, 129.3, 127.2, 121.5, 115.5, 113.5, 78.4, 55.3, 44.3, 34.5, 29.2, 28.1; ESI-MS m/z calculated for $C_{28}H_{39}N_3O_4^+$ $[M + 2H]^+$ 481.6; found 481.7.

tert-Butyl 5-(4-(4-Methoxybenzamido)phenyl)-2,5-diazabicyclo[2.2.1]heptane-2-carboxylate (2g). 2g was synthesized using 1a (176 mg, 0.5 mmol) and *tert*-butyl 2,5-diazabicyclo[2.2.1]heptane-2-carboxylate (109 mg, 0.55 mmol) in general procedure A to afford 2g (112 mg, 53% yield) as a white solid. (1H NMR, 400 MHz, DMSO- d_6): δ = 9.81 (s, 1H), 7.89 (d, J = 8.8 Hz, 2H), 7.54 (d, J = 8.3 Hz, 2H), 7.03 (d, J = 8.9 Hz, 2H), 6.59 (d, J = 9.0 Hz, 2H), 4.46 (d, J = 4.7 Hz, 1H), 4.40 (d, J = 23.6 Hz, 1H), 3.83 (s, 3H), 3.54 (t, J = 8.8 Hz, 1H), 3.30–3.21 (m, 2H), 2.95 (t, J = 7.6 Hz, 1H), 1.91 (s + d, J = 9.4 Hz, 2H), 1.36 (d, J = 12.5 Hz, 9H); (^{13}C NMR, 100 MHz, DMSO- d_6): δ = 164.1, 161.6, 153.5, 153.2, 143.4, 129.3, 128.9, 128.8, 127.3, 122.1, 122.0, 113.5, 112.4, 78.6, 78.5, 59.7, 57.4, 57.0, 56.9, 56.8, 56.2, 56.0, 55.3, 50.8, 50.6, 37.1, 36.5, 28.1, 28.0, 20.7, 14.0; ESI-MS m/z calculated for $C_{24}H_{30}N_3O_4^+$ $[M + H]^+$ 424.5; found 424.6.

tert-Butyl 8-(4-(4-Methoxybenzamido)phenyl)-3,8-diazabicyclo[3.2.1]octane-3-carboxylate (2h). 2h was synthesized using 1a (2 g, 5.66 mmol) and *tert*-butyl 3,8-diazabicyclo[3.2.1]octane-3-carboxylate (1.3 g, 6.2 mmol) in general procedure A to afford 2h (2.1 g, 86% yield) as a white solid. (1H NMR, 400 MHz, MeOD): δ = 7.89 (dt, J_1 = 8.8 Hz, J_2 = 2.8 Hz, 2H), 7.49 (d, J = 8.9 Hz, 2H), 7.01 (dt, J_1 = 8.8 Hz, J_2 = 2.9 Hz, 2H), 6.89 (dt, J_1 = 9.0 Hz, J_2 = 3.1 Hz, 2H), 4.22 (d, J = 12.2 Hz, 2H), 3.86 (s, 3H), 3.66 (d, J = 12.6 Hz, 2H), 3.27 (d, J = 12.6 Hz, 1H), 3.17 (d, J = 12.5 Hz, 1H), 2.00 (t, J = 5.8 Hz, 2H), 1.80 (q, J = 6.4 Hz, 2H), 1.46 (s, 9H); (^{13}C NMR, 100 MHz, MeOD): δ = 168.3, 164.1, 158.0, 145.4, 131.0, 130.6, 128.4, 124.6, 117.2, 114.9, 81.4, 56.1, 28.8, 27.9; ESI-MS m/z calculated for $C_{25}H_{32}N_3O_4^+$ $[M + H]^+$ 438.5; found 438.3.

tert-Butyl 9-(4-(4-Methoxybenzamido)phenyl)-3,9-diazabicyclo[3.3.1]nonane-3-carboxylate (2i). 2i was synthesized using 1a (200 mg, 0.57 mmol) and *tert*-butyl 3,9-diazabicyclo[3.3.1]nonane-3-carboxylate (140 mg, 0.62 mmol) in general procedure A to afford 2i (73 mg, 28% yield) as a white waxy solid. (1H NMR, 400 MHz, CD $_3$ CN): δ = 8.47 (s, 1H), 7.88 (dt, J_1 = 8.9 Hz, J_2 = 2.9 Hz, 2H), 7.53 (dt, J_1 = 9.0 Hz, J_2 = 3.3 Hz, 2H), 7.02 (dt, J_1 = 8.9 Hz, J_2 = 3.0 Hz, 2H), 6.89 (dt, J_1 = 9.1 Hz, J_2 = 3.3 Hz, 2H), 4.24 (d, J = 11.2 Hz, 2H), 3.85 (s, 3H), 3.64 (dd, J_1 = 11.4 Hz, J_2 = 5.2 Hz, 2H), 2.95–2.90 (m, 2H), 2.49–2.36 (m, 1H), 1.81 (dd, J_1 = 8.8 Hz, J_2 = 3.1 Hz, 4H), 1.52 (dt, J_1 = 13.2 Hz, J_2 = 3.8 Hz, 1H), 1.45 (s, 9H); (^{13}C NMR, 100 MHz, CD $_3$ CN): δ = 165.9, 163.3, 154.8, 148.6, 131.5, 130.2, 128.5, 123.1, 116.1, 114.7, 80.0, 56.3, 53.4, 53.3, 49.1, 47.5, 30.7, 30.2, 28.7, 20.5; ESI-MS m/z calculated for $C_{26}H_{34}N_3O_4^+$ $[M + H]^+$ 452.6; found 452.6.

tert-Butyl 4-(4-(4-Methoxybenzamido)phenyl)-1,4-diazepane-1-carboxylate (2j). 2j was synthesized using 1a (202 mg, 0.57 mmol) and *tert*-butyl 1,4-diazepane-1-carboxylate (126 mg, 0.63 mmol) in general procedure A to afford 2j (125 mg, 52% yield) as a colorless oil. (1H NMR, 400 MHz, DMSO- d_6): δ = 9.76 (s, 1H), 7.93 (d, J = 8.8 Hz, 2H), 7.53 (d, J = 5.9 Hz, 2H), 7.03 (d, J = 8.8 Hz, 2H), 6.70 (q, J = 4.3 Hz, 2H), 3.83 (s, 3H), 3.54–3.48 (m, 6H), 3.22 (t, J = 5.3 Hz, 1H), 3.15 (t, J = 5.5 Hz, 1H), 1.86 (t, J = 5.4 Hz, 1H), 1.80 (t, J = 6.1 Hz, 1H), 1.31 (d, J = 38.0 Hz, 9H); (^{13}C NMR, 100 MHz, DMSO- d_6): δ = 164.0, 161.5, 154.4, 154.1, 143.5, 143.4, 129.3, 127.3, 122.2, 122.0, 113.4, 111.3, 78.4, 55.3, 54.9, 49.5, 49.0, 48.2, 47.6, 45.4, 45.2, 45.0, 28.0, 27.8, 25.0, 24.6; ESI-MS m/z calculated for $C_{24}H_{32}N_3O_4^+$ $[M + H]^+$ 426.5; found 426.6.

tert-Butyl 4-(6-(4-Methoxybenzamido)pyridin-3-yl)piperazine-1-carboxylate (2k). 2k was synthesized using 1b (100 mg, 0.33 mmol) and *tert*-butyl piperazine-1-carboxylate (61 mg, 0.33 mmol) in general

procedure A to afford 2k (120 mg, 88% yield) as a white solid. (1H NMR, 400 MHz, DMSO- d_6): δ = 10.40 (s, 1H), 8.08 (d, J = 2.8 Hz, 1H), 8.02 (d, J = 8.8 Hz, 3H), 7.46 (dd, J_1 = 9.1 Hz, J_2 = 2.9 Hz, 1H), 7.02 (d, J = 8.8 Hz, 2H), 3.83 (s, 3H), 3.48 (t, J = 4.6 Hz, 4H), 3.12 (t, J = 5.0 Hz, 4H), 1.42 (s, 9H); (^{13}C NMR, 100 MHz, DMSO- d_6): δ = 164.6, 161.9, 153.8, 144.9, 143.6, 135.7, 129.7, 126.3, 125.4, 115.1, 113.5, 79.0, 55.4, 48.4, 28.0; ESI-MS m/z calculated for $C_{22}H_{30}N_4O_4^+$ $[M + 2H]^+$ 414.5; found 414.4.

tert-Butyl 8-(6-(4-Methoxybenzamido)pyridin-3-yl)-3,8-diazabicyclo[3.2.1]octane-3-carboxylate (2l). 2l was synthesized using 1b (200 mg, 0.65 mmol) and *tert*-butyl 3,8-diazabicyclo[3.2.1]octane-3-carboxylate (152 mg, 0.65 mmol) in general procedure A to afford 2l (160 mg, 56% yield) as a white waxy solid. (1H NMR, 400 MHz, CDCl $_3$): δ = 10.01 (s, 1H), 8.52 (d, J = 9.3 Hz, 1H), 8.04 (d, J = 8.8 Hz, 2H), 7.67 (d, J = 2.5 Hz, 1H), 7.40 (dd, J_1 = 9.4 Hz, J_2 = 2.8 Hz, 1H), 6.97 (d, J = 8.9 Hz, 2H), 4.12 (d, J = 23.9 Hz, 2H), 3.85 (s, 3H), 3.80 (d, J = 12.2 Hz, 1H), 3.65 (d, J = 13.3 Hz, 1H), 3.23 (d, J = 12.4 Hz, 1H), 3.12 (d, J = 12.7 Hz, 1H), 2.02 (s, 2H), 1.87 (q, J = 7.4 Hz, 2H), 1.43 (s, 9H); (^{13}C NMR, 100 MHz, CDCl $_3$): δ = 165.2, 163.3, 156.0, 142.5, 140.1, 129.9, 129.2, 125.6, 117.0, 114.3, 114.2, 80.4, 77.4, 55.7, 28.6; ESI-MS m/z calculated for $C_{24}H_{32}N_4O_4^+$ $[M + 2H]^+$ 440.5; found 440.4.

tert-Butyl 4-(6-(4-Methoxybenzamido)pyridin-3-yl)-1,4-diazepane-1-carboxylate (2m). 2m was synthesized using 1b (200 mg, 0.65 mmol) and *tert*-butyl 1,4-diazepane-1-carboxylate (144 mg, 0.72 mmol) in general procedure A to afford 2m (162 mg, 58% yield) as a light brown oil. (1H NMR, 400 MHz, MeOD): δ = 7.94 (q, J = 7.3 Hz, 3H), 7.86 (s, 1H), 7.27 (dd, J_1 = 9.1 Hz, J_2 = 2.9 Hz, 1H), 7.04 (d, J = 8.8 Hz, 2H), 3.88 (s, 3H), 3.67–3.60 (m, 6H), 3.33 (s, 2H), 1.96–1.90 (m, 2H), 1.35 (d, J = 30.8 Hz, 9H); (^{13}C NMR, 100 MHz, MeOD): δ = 166.2, 162.9, 155.6, 155.4, 141.2, 130.9, 129.1, 126.3, 121.0, 120.9, 116.5, 116.4, 113.5, 79.7, 79.6, 54.6, 45.2, 45.1, 27.2, 27.1, 24.6, 24.3; ESI-MS m/z calculated for $C_{23}H_{32}N_4O_4^+$ $[M + 2H]^+$ 428.5; found 428.5.

tert-Butyl 8-(5-(4-Methoxybenzamido)pyridin-2-yl)-3,8-diazabicyclo[3.2.1]octane-3-carboxylate (2n). 2n was synthesized using 1c (200 mg, 0.65 mmol) and *tert*-butyl 3,8-diazabicyclo[3.2.1]octane-3-carboxylate (152 mg, 0.72 mmol) in general procedure A to afford 2n (74 mg, 26% yield) as a white solid. (1H NMR, 400 MHz, DMSO- d_6): δ = 9.96 (s, 1H), 8.43 (d, J = 2.6 Hz, 1H), 7.94 (dt, J_1 = 8.8 Hz, J_2 = 2.8 Hz, 2H), 7.89 (dd, J_1 = 9.0 Hz, J_2 = 2.6 Hz, 1H), 7.05 (dt, J_1 = 8.9 Hz, J_2 = 2.8 Hz, 2H), 6.84 (d, J = 9.0 Hz, 1H), 4.52 (s, 2H), 3.83 (s, 3H), 3.64 (q, J = 12.1 Hz, 2H), 3.12 (d, J = 12.4 Hz, 1H), 2.98 (d, J = 11.8 Hz, 1H), 1.88 (t, J = 3.8 Hz, 2H), 1.67 (t, J = 6.8 Hz, 2H), 1.40 (s, 9H); (^{13}C NMR, 100 MHz, DMSO- d_6): δ = 164.6, 161.8, 155.2, 153.7, 140.9, 131.4, 129.4, 126.8, 126.7, 113.6, 108.6, 78.8, 55.4, 54.9, 28.0; ESI-MS m/z calculated for $C_{24}H_{31}N_4O_4^+$ $[M + H]^+$ 439.5; found 439.5.

N-(4-(2,6-Diazaspiro[3.3]heptan-2-yl)phenyl)-4-methoxybenzamide (3a). 3a was synthesized using 2a (100 mg, 0.24 mmol) in general procedure B to afford 3a (88 mg, 100% yield) as a white solid. (1H NMR, 400 MHz, MeOD): δ = 7.88 (d, J = 8.8 Hz, 2H), 7.45 (d, J = 8.8 Hz, 2H), 7.00 (dt, J_1 = 8.9 Hz, J_2 = 2.8 Hz, 2H), 6.51 (d, J = 8.8 Hz, 2H), 4.15 (s, 4H), 3.99 (s, 4H), 3.86 (s, 3H); (^{13}C NMR, 100 MHz, MeOD): δ = 168.4, 164.2, 150.3, 131.3, 130.5, 128.4, 124.2, 114.9, 113.4, 63.1, 57.1, 56.1, 38.5; ESI-MS m/z calculated for $C_{19}H_{22}N_3O_2^+$ $[M + H]^+$ 324.4; found 324.4.

N-(4-(2,7-Diazaspiro[3.5]nonan-2-yl)phenyl)-4-methoxybenzamide (3b). 3b was synthesized using 2b (350 mg, 0.78 mmol) in general procedure B to afford 3b (218 mg, 80% yield) as a white solid. (1H NMR, 400 MHz, MeOD): δ = 7.88 (d, J = 8.8 Hz, 2H), 7.42 (d, J = 8.8 Hz, 2H), 7.00 (dt, J_1 = 8.9 Hz, J_2 = 2.9 Hz, 2H), 6.49 (t, J_1 = 8.9 Hz, J_2 = 2.9 Hz, 2H), 3.85 (s, 3H), 3.59 (s, 4H), 2.78 (t, J = 5.4 Hz, 4H), 1.78 (t, J = 5.6 Hz, 4H); (^{13}C NMR, 100 MHz, MeOD): δ = 168.4, 164.1, 151.1, 130.5, 130.4, 128.5, 124.3, 114.9, 112.9, 63.8, 56.1, 44.1, 37.4, 35.9; ESI-MS m/z calculated for $C_{21}H_{26}N_3O_2^+$ $[M + H]^+$ 352.5; found 352.5.

N-(4-(2,7-Diazaspiro[4.4]nonan-2-yl)phenyl)-4-methoxybenzamide (3c). 3c was synthesized using 2c (65 mg, 0.14 mmol) in general procedure B to afford 3c (36 mg, 71% yield) as a white solid. (1H NMR, 400 MHz, DMSO- d_6): δ = 9.77 (s, 1H), 7.93 (d, J = 8.8 Hz, 2H), 7.52 (d, J = 8.9 Hz, 2H), 7.03 (dt, J_1 = 8.9 Hz, J_2 = 2.7 Hz, 2H), 6.48 (d, J =

9.0 Hz, 2H), 3.83 (s, 3H), 3.30–3.26 (m, 2H), 3.20 (d, $J = 9.2$ Hz, 1H), 3.14 (d, $J = 9.2$ Hz, 1H), 2.92 (t, $J = 7.1$ Hz, 2H), 2.75 (dd, $J_1 = 12.8$ Hz, $J_2 = 10.9$ Hz, 2H), 1.96–1.88 (m, 2H), 1.77–1.69 (m, 2H); (^{13}C NMR, 100 MHz, DMSO- d_6): $\delta = 164.0, 161.5, 144.5, 129.3, 128.0, 127.3, 122.2, 113.5, 111.0, 57.8, 56.6, 55.4, 54.9, 49.2, 47.2, 45.7, 36.7, 35.6$; ESI-MS m/z calculated for $\text{C}_{21}\text{H}_{26}\text{N}_3\text{O}_2^+ [\text{M} + \text{H}]^+$ 352.5; found 352.5.

N-(4-(Hexahydropyrrolo[3,4-b]pyrrol-1(2H)-yl)phenyl)-4-methoxybenzamide (3d). 3d was synthesized using 2d (100 mg, 0.29 mmol) in general procedure B to afford 3d (68 mg, 69% yield) as a white solid. (^1H NMR, 400 MHz, DMSO- d_6): $\delta = 9.79$ (s, 1H), 7.93 (d, $J = 8.8$ Hz, 2H), 7.52 (d, $J = 8.9$ Hz, 2H), 7.03 (d, $J = 8.8$ Hz, 2H), 6.53 (d, $J = 8.9$ Hz, 2H), 3.92 (t, $J = 5.5$ Hz, 1H), 3.83 (s, 3H), 3.08 (q, $J = 7.4$ Hz, 1H), 2.88–2.66 (m, 6H), 2.10–2.02 (m, 1H), 1.79–1.71 (m, 1H); (^{13}C NMR, 100 MHz, DMSO- d_6): $\delta = 161.6, 129.3, 128.5, 127.3, 122.1, 113.5, 112.3, 65.0, 55.4, 52.6, 48.9, 29.6$; ESI-MS m/z calculated for $\text{C}_{20}\text{H}_{25}\text{N}_3\text{O}_2^+ [\text{M} + 2\text{H}]^+$ 339.4; found 339.4.

N-(4-(2,8-Diazaspiro[4.5]decan-8-yl)phenyl)-4-methoxybenzamide (3e). 3e was synthesized using 2e (40 mg, 0.09 mmol) in general procedure B to afford 3e (25 mg, 80% yield) as a white solid. (^1H NMR, 400 MHz, DMSO- d_6): $\delta = 9.87$ (s, 1H), 7.94 (dt, $J_1 = 8.8$ Hz, $J_2 = 2.8$ Hz, 2H), 7.58 (d, $J = 9.0$ Hz, 2H), 7.04 (dt, $J_1 = 8.9$ Hz, $J_2 = 2.8$ Hz, 2H), 6.92 (d, $J = 9.1$ Hz, 2H), 3.83 (s, 3H), 3.09 (q, $J = 5.6$ Hz, 4H), 2.86 (t, $J = 7.0$ Hz, 2H), 2.63 (s, 2H), 1.59 (t, $J = 5.6$ Hz, 4H), 1.54 (t, $J = 7.1$ Hz, 2H); (^{13}C NMR, 100 MHz, DMSO- d_6): $\delta = 164.3, 161.6, 147.7, 130.8, 129.4, 127.2, 121.5, 115.9, 113.5, 57.3, 55.4, 47.0, 45.3, 37.1, 35.3, 30.7$; ESI-MS m/z calculated for $\text{C}_{22}\text{H}_{28}\text{N}_3\text{O}_2^+ [\text{M} + \text{H}]^+$ 366.5; found 366.5.

N-(4-(3,9-Diazaspiro[5.5]undecan-3-yl)phenyl)-4-methoxybenzamide (3f). 3f was synthesized using 2f (185 mg, 0.39 mmol) in general procedure B to afford 3f (120 mg, 81% yield) as a white solid. (^1H NMR, 400 MHz, MeOD): $\delta = 7.89$ (dt, $J_1 = 8.9$ Hz, $J_2 = 2.8$ Hz, 2H), 7.51 (d, $J = 9.0$ Hz, 2H), 7.00 (tt, $J_1 = 8.6$ Hz, $J_2 = 2.8$ Hz, 4H), 3.86 (s, 3H), 3.15 (t, $J = 5.6$ Hz, 4H), 3.00 (t, $J = 5.7$ Hz, 4H), 1.71 (t, $J = 5.7$ Hz, 4H), 1.64 (t, $J = 5.8$ Hz, 4H); (^{13}C NMR, 100 MHz, MeOD): $\delta = 168.4, 164.2, 150.3, 132.5, 130.6, 128.4, 123.8, 118.2, 114.9, 56.1, 46.9, 41.8, 36.6, 35.3, 30.4$; ESI-MS m/z calculated for $\text{C}_{23}\text{H}_{30}\text{N}_3\text{O}_2^+ [\text{M} + \text{H}]^+$ 380.5; found 380.5.

N-(4-(2,5-Diazabicyclo[2.2.1]heptan-2-yl)phenyl)-4-methoxybenzamide (3g). 3g was synthesized using 2g (100 mg, 0.24 mmol) in general procedure B to afford 3g (76 mg, 100% yield) as a white solid. (^1H NMR, 400 MHz, DMSO- d_6): $\delta = 9.79$ (s, 1H), 7.94 (d, $J = 8.8$ Hz, 2H), 7.51 (d, $J = 8.8$ Hz, 2H), 7.04 (d, $J = 8.9$ Hz, 2H), 6.54 (d, $J = 8.9$ Hz, 2H), 4.29 (s, 1H), 3.08 (s, 3H), 3.60 (s, 1H), 3.49 (dd, $J_1 = 8.4$ Hz, $J_2 = 2.0$ Hz, 1H), 2.88–2.81 (m, 3H), 1.78 (d, $J = 9.2$ Hz, 1H), 1.64 (d, $J = 9.0$ Hz, 1H); (^{13}C NMR, 100 MHz, DMSO- d_6): $\delta = 164.1, 161.5, 144.0, 129.3, 128.2, 127.3, 122.1, 113.5, 112.3, 59.2, 56.6, 55.8, 55.4, 48.9, 37.1$; ESI-MS m/z calculated for $\text{C}_{19}\text{H}_{22}\text{N}_3\text{O}_2^+ [\text{M} + \text{H}]^+$ 324.4; found 324.3.

N-(4-(3,8-Diazabicyclo[3.2.1]octan-8-yl)phenyl)-4-methoxybenzamide (3h). 3h was synthesized using 2h (1.9 g, 4.3 mmol) in general procedure B to afford 3h (1.2 g, 85% yield) as a white solid. (^1H NMR, 400 MHz, DMSO- d_6): $\delta = 9.80$ (s, 1H), 7.93 (d, $J = 8.8$ Hz, 2H), 7.55 (dd, $J_1 = 9.0$ Hz, $J_2 = 3.1$ Hz, 2H), 7.04 (d, $J = 8.8$ Hz, 2H), 6.76 (d, $J = 9.0$ Hz, 2H), 4.04 (s, 2H), 3.83 (s, 3H), 3.03 (s, 1H), 2.96 (d, $J = 11.9$ Hz, 2H), 2.38 (d, $J = 11.2$ Hz, 2H), 1.93–1.84 (m, 4H); (^{13}C NMR, 100 MHz, DMSO- d_6): $\delta = 164.2, 161.6, 143.8, 129.3, 128.8, 127.3, 122.2, 122.1, 55.7, 55.3, 47.0, 26.8$; ESI-MS m/z calculated for $\text{C}_{20}\text{H}_{24}\text{N}_3\text{O}_2^+ [\text{M} + \text{H}]^+$ 338.4; found 338.4.

N-(4-(3,9-Diazabicyclo[3.3.1]nonan-9-yl)phenyl)-4-methoxybenzamide (3i). 3i was synthesized using 2i (65 mg, 0.14 mmol) in general procedure B to afford 3i (40 mg, 79% yield) as a white solid. (^1H NMR, 400 MHz, DMSO- d_6): $\delta = 9.85$ (s, 1H), 7.94 (dt, $J_1 = 8.8$ Hz, $J_2 = 2.8$ Hz, 2H), 7.58 (d, $J = 9.0$ Hz, 2H), 7.04 (dt, $J_1 = 8.9$ Hz, $J_2 = 2.8$ Hz, 2H), 6.85 (d, $J = 9.1$ Hz, 2H), 3.84 (s, 3H), 4.59 (d, $J = 11.0$ Hz, 2H), 3.11 (s, 2H), 2.92 (dd, $J_1 = 11.3$ Hz, $J_2 = 2.7$ Hz, 2H), 2.31–2.23 (m, 1H), 1.86–1.72 (m, 4H), 1.50 (t, $J = 6.8$ Hz, 1H); (^{13}C NMR, 100 MHz, DMSO- d_6): $\delta = 164.2, 161.6, 147.2, 130.0, 129.3, 127.2, 121.6, 113.8, 113.5, 55.4, 54.9, 52.5, 46.7, 30.9, 19.9$; ESI-MS m/z calculated for $\text{C}_{21}\text{H}_{27}\text{N}_3\text{O}_2^+ [\text{M} + 2\text{H}]^+$ 353.5; found 353.5.

N-(4-(1,4-Diazepan-1-yl)phenyl)-4-methoxybenzamide (3j). 3j was synthesized using 2j (111 mg, 0.26 mmol) in general procedure

B to afford 3j (65 mg, 77% yield) as a yellow oil. (^1H NMR, 400 MHz, DMSO- d_6): $\delta = 9.76$ (s, 1H), 7.92 (dt, $J_1 = 8.8$ Hz, $J_2 = 2.9$ Hz, 2H), 7.49 (d, $J = 9.0$ Hz, 2H), 7.03 (dt, $J_1 = 8.8$ Hz, $J_2 = 2.9$ Hz, 2H), 6.66 (d, $J = 9.2$ Hz, 2H), 3.83 (s, 3H), 3.51 (t, $J = 6.1$ Hz, 2H), 3.44 (t, $J = 5.0$ Hz, 2H), 2.86 (t, $J = 5.2$ Hz, 2H), 2.64 (t, $J = 5.7$ Hz, 2H), 1.82–1.76 (m, 2H); (^{13}C NMR, 100 MHz, DMSO- d_6): $\delta = 164.1, 161.5, 144.9, 129.3, 127.7, 127.3, 122.4, 113.5, 111.0, 55.4, 54.9, 51.8, 47.3, 47.2, 28.8$; ESI-MS m/z calculated for $\text{C}_{19}\text{H}_{25}\text{N}_3\text{O}_2^+ [\text{M} + 2\text{H}]^+$ 327.4; found 327.4.

4-Methoxy-N-(5-(piperazin-1-yl)pyridin-2-yl)benzamide (3k). 3k was synthesized using 2k (100 mg, 0.24 mmol) in general procedure B to afford 3k (66 mg, 88% yield) as a white solid. (^1H NMR, 400 MHz, MeOD): $\delta = 8.03$ (d, $J = 9.4$ Hz, 2H), 7.95 (d, $J = 8.8$ Hz, 2H), 7.48 (dd, $J_1 = 9.0$ Hz, $J_2 = 3.0$ Hz, 1H), 7.05 (d, $J = 8.8$ Hz, 2H), 3.89 (s, 3H), 3.18 (t, $J = 4.7$ Hz, 4H), 3.00 (t, $J = 4.8$ Hz, 4H); (^{13}C NMR, 100 MHz, MeOD): $\delta = 167.9, 164.5, 146.6, 145.9, 137.0, 130.7, 127.8, 127.2, 117.2, 115.1, 56.1, 50.8, 46.5$; ESI-MS m/z calculated for $\text{C}_{17}\text{H}_{22}\text{N}_4\text{O}_2^+ [\text{M} + 2\text{H}]^+$ 314.4; found 314.3.

N-(5-(3,8-Diazabicyclo[3.2.1]octan-8-yl)pyridin-2-yl)-4-methoxybenzamide (3l). 3l was synthesized using 2l (152 mg, 0.35 mmol) in general procedure B to afford 3l (120 mg, 100% yield) as a white solid. (^1H NMR, 400 MHz, MeOD): $\delta = 7.98$ –7.92 (m, 4H), 7.38 (dd, $J_1 = 9.1$ Hz, $J_2 = 3.0$ Hz, 1H), 7.04 (dt, $J_1 = 8.9$ Hz, $J_2 = 2.9$ Hz, 2H), 4.24 (s, 2H), 3.87 (s, 3H), 3.17 (d, $J = 12.4$ Hz, 2H), 2.72 (d, $J = 12.4$ Hz, 2H), 2.13–2.08 (m, 2H), 2.03 (q, $J = 7.8$ Hz, 2H); (^{13}C NMR, 100 MHz, MeOD): $\delta = 167.9, 164.5, 144.3, 142.2, 136.3, 130.7, 127.8, 126.4, 118.1, 115.1, 56.8, 56.2, 47.7, 27.6$; ESI-MS m/z calculated for $\text{C}_{19}\text{H}_{23}\text{N}_4\text{O}_2^+ [\text{M} + \text{H}]^+$ 339.4; found 339.4.

N-(5-(1,4-Diazepan-1-yl)pyridin-2-yl)-4-methoxybenzamide (3m). 3m was synthesized using 2m (140 mg, 0.33 mmol) in general procedure B to afford 3m (80 mg, 74% yield) as a white solid. (^1H NMR, 400 MHz, MeOD): $\delta = 7.94$ (d, $J = 8.8$ Hz, 2H), 7.89 (d, $J = 9.1$ Hz, 1H), 7.87 (d, $J = 3.0$ Hz, 1H), 7.27 (dd, $J_1 = 9.1$ Hz, $J_2 = 3.1$ Hz, 1H), 7.05 (d, $J = 8.8$ Hz, 2H), 3.89 (s, 3H), 3.62 (q, $J = 5.8$ Hz, 4H), 3.04 (t, $J = 5.3$ Hz, 2H), 2.85 (t, $J = 5.6$ Hz, 2H), 2.01–1.95 (m, 2H); (^{13}C NMR, 100 MHz, MeOD): $\delta = 167.8, 164.4, 144.0, 142.5, 132.2, 130.6, 127.8, 122.2, 118.3, 115.0, 56.1, 51.9, 48.8, 29.9$; ESI-MS m/z calculated for $\text{C}_{18}\text{H}_{23}\text{N}_4\text{O}_2^+ [\text{M} + \text{H}]^+$ 327.4; found 327.4.

N-(6-(3,8-Diazabicyclo[3.2.1]octan-8-yl)pyridin-3-yl)-4-methoxybenzamide (3n). 3n was synthesized using 2n (64 mg, 0.15 mmol) in general procedure B to afford 3n (48 mg, 97% yield) as a colorless oil. (^1H NMR, 400 MHz, DMSO- d_6): $\delta = 8.34$ (s, 1H), 7.92 (d, $J = 8.3$ Hz, 2H), 7.85 (d, $J = 9.0$ Hz, 1H), 7.03 (d, $J = 8.4$ Hz, 2H), 6.79 (d, $J = 9.0$ Hz, 1H), 4.41 (s, 2H), 3.87 (s, 3H), 3.05 (d, $J = 12.8$ Hz, 2H), 2.63 (d, $J = 12.8$ Hz, 2H), 2.09–1.99 (m, 2H); (^{13}C NMR, 100 MHz, DMSO- d_6): $\delta = 159.0, 154.7, 146.6, 133.1, 124.6, 121.0, 118.3, 117.5, 105.3, 100.8, 47.1, 46.5, 18.3$; ESI-MS m/z calculated for $\text{C}_{19}\text{H}_{23}\text{N}_4\text{O}_2^+ [\text{M} + \text{H}]^+$ 339.4; found 339.4.

4-Methoxy-N-(4-(6-(pyridin-2-yl)-2,6-diazaspiro[3.3]heptan-2-yl)phenyl)benzamide (4a). 4a was synthesized using 3a (60 mg, 0.19 mmol) in general procedure C to afford 4a (30 mg, 40% yield) as a white solid. (^1H NMR, 400 MHz, DMSO- d_6): $\delta = 9.83$ (s, 1H), 8.07 (dd, $J_1 = 5.0$ Hz, $J_2 = 1.0$ Hz, 1H), 7.93 (d, $J = 8.8$ Hz, 2H), 7.55 (d, $J = 8.8$ Hz, 2H), 7.03 (ddd, $J_1 = 8.2$ Hz, $J_2 = 7.1$ Hz, $J_3 = 1.9$ Hz, 1H), 7.03 (d, $J = 8.8$ Hz, 2H), 6.64 (dd, $J_1 = 6.8$ Hz, $J_2 = 5.2$ Hz, 1H), 6.45 (d, $J = 8.8$ Hz, 2H), 6.39 (d, $J = 8.3$ Hz, 1H), 4.10 (s, 4H), 3.96 (s, 4H), 3.83 (s, 3H); (^{13}C NMR, 100 MHz, DMSO- d_6): $\delta = 164.2, 161.6, 160.4, 148.1, 147.7, 137.0, 129.9, 129.3, 127.2, 121.8, 113.5, 112.9, 111.5, 106.0, 62.1, 60.5, 55.3, 34.1$; ESI-MS m/z calculated for $\text{C}_{24}\text{H}_{26}\text{N}_4\text{O}_2^+ [\text{M} + 2\text{H}]^+$ 402.5; found 402.7; HRMS (ESI) for $\text{C}_{24}\text{H}_{25}\text{N}_4\text{O}_2^+ [\text{M} + \text{H}]^+$ 401.1978; found 401.1979.

4-Methoxy-N-(4-(7-(pyridin-2-yl)-2,7-diazaspiro[3.5]nonan-2-yl)phenyl)benzamide (4b). 4b was synthesized using 3b (112 mg, 0.32 mmol) in general procedure C to afford 4b (103 mg, 75% yield) as a white solid. (^1H NMR, 400 MHz, DMSO- d_6): $\delta = 9.81$ (s, 1H), 8.10 (dd, $J_1 = 4.8$ Hz, $J_2 = 1.4$ Hz, 1H), 7.93 (dt, $J_1 = 8.8$ Hz, $J_2 = 2.8$ Hz, 2H), 7.53 (d, $J = 8.8$ Hz, 2H), 7.50 (ddd, $J_1 = 8.7$ Hz, $J_2 = 6.9$ Hz, $J_3 = 2.0$ Hz, 1H), 7.03 (dt, $J_1 = 8.9$ Hz, $J_2 = 2.9$ Hz, 2H), 6.84 (d, $J = 8.6$ Hz, 1H), 6.59 (dd, $J_1 = 6.8$ Hz, $J_2 = 5.3$ Hz, 1H), 6.42 (d, $J = 8.9$ Hz, 2H), 3.83 (s, 3H), 3.59 (s, 4H), 3.53 (t, $J = 5.3$ Hz, 4H), 1.78 (t, $J = 5.4$ Hz, 4H); (^{13}C NMR, 100 MHz, DMSO- d_6): $\delta = 164.2, 161.6, 158.8, 148.4, 147.6,$

137.4, 129.4, 129.3, 127.2, 121.9, 113.5, 112.4, 111.0, 107.1, 61.6, 55.3, 42.0, 34.7, 34.5; ESI-MS m/z calculated for $C_{26}H_{30}N_4O_2^+$ [M + 2H]⁺ 430.6; found 430.6; HRMS (ESI) for $C_{26}H_{29}N_4O_2^+$ [M + H]⁺ 429.2291; found 429.2278.

4-Methoxy-N-(4-(7-(3-nitrophenyl)-2,7-diazaspiro[3.5]nonan-2-yl)phenyl)benzamide (4c). 4c was synthesized using 3b (123 mg, 0.35 mmol) in general procedure C to afford 4c (97 mg, 59% yield) as a yellow solid. (¹H NMR, 400 MHz, DMSO-*d*₆): δ = 9.82 (s, 1H), 7.94 (d, *J* = 8.8 Hz, 2H), 7.68 (t, *J* = 2.2 Hz, 1H), 7.57–7.53 (m, 3H), 7.49–7.43 (m, 2H), 7.04 (d, *J* = 8.9 Hz, 2H), 6.43 (d, *J* = 8.8 Hz, 2H), 3.83 (s, 3H), 3.61 (s, 4H), 3.33 (t, *J* = 5.4 Hz, 4H+water), 1.88 (t, *J* = 5.3 Hz, 4H); (¹³C NMR, 100 MHz, DMSO-*d*₆): δ = 164.2, 161.6, 151.5, 148.9, 148.4, 130.1, 129.4, 129.3, 127.2, 121.9, 121.7, 113.5, 112.3, 111.0, 108.6, 61.5, 55.3, 45.2, 34.5, 34.0; ESI-MS m/z calculated for $C_{27}H_{29}N_4O_4^+$ [M + H]⁺ 473.6; found 473.6; HRMS (ESI) for $C_{27}H_{29}N_4O_4^+$ [M + H]⁺ 473.2189; found 473.2167.

4-Methoxy-N-(4-(7-(pyridin-2-yl)-2,7-diazaspiro[4.4]nonan-2-yl)phenyl)benzamide (4d). 4d was synthesized using 3c (27 mg, 0.08 mmol) in general procedure C to afford 4d (9 mg, 26% yield) as a yellow solid. (¹H NMR, 400 MHz, DMSO-*d*₆): δ = 9.79 (s, 1H), 8.05 (dd, *J*₁ = 4.9 Hz, *J*₂ = 1.3 Hz, 1H), 7.94 (dt, *J*₁ = 8.8 Hz, *J*₂ = 2.9 Hz, 2H), 7.54 (d, *J* = 8.9 Hz, 2H), 7.47 (ddd, *J*₁ = 8.6 Hz, *J*₂ = 6.9 Hz, *J*₃ = 2.0 Hz, 1H), 7.03 (dt, *J*₁ = 8.8 Hz, *J*₂ = 2.9 Hz, 2H), 6.55–6.51 (m, 3H), 6.44 (d, *J* = 8.5 Hz, 1H), 3.83 (s, 3H), 3.51 (t, *J* = 7.0 Hz, 2H), 3.46–3.35 (m, 4H), 3.26 (dd, *J*₁ = 12.2 Hz, *J*₂ = 9.4 Hz, 2H), 2.07–1.97 (m, 4H); (¹³C NMR, 100 MHz, DMSO-*d*₆): δ = 164.0, 161.5, 156.9, 147.8, 144.4, 136.9, 129.3, 128.1, 127.3, 122.1, 113.4, 111.2, 106.2, 57.2, 56.0, 55.3, 54.9, 48.0, 47.0, 45.7, 34.8, 34.7; ESI-MS m/z calculated for $C_{26}H_{30}N_4O_2^+$ [M + 2H]⁺ 430.5; found 430.5; HRMS (ESI) for $C_{26}H_{29}N_4O_2^+$ [M + H]⁺ 429.2291; found 429.2285.

4-Methoxy-N-(4-(5-(pyridin-2-yl)hexahydropyrrolo[3,4-*b*]pyrrol-1(2H)-yl)phenyl)benzamide (4e). 4e was synthesized using 3d (24 mg, 0.06 mmol) in general procedure C to afford 4e (18 mg, 79% yield) as a white solid. (¹H NMR, 400 MHz, DMSO-*d*₆): δ = 9.83 (s, 1H), 8.05 (dd, *J*₁ = 4.9 Hz, *J*₂ = 1.3 Hz, 1H), 7.95 (dt, *J*₁ = 8.8 Hz, *J*₂ = 2.8 Hz, 2H), 7.57 (d, *J* = 8.9 Hz, 2H), 7.47 (ddd, *J*₁ = 8.6 Hz, *J*₂ = 7.0 Hz, *J*₃ = 2.0 Hz, 1H), 7.04 (dt, *J*₁ = 8.9 Hz, *J*₂ = 2.8 Hz, 2H), 6.59–6.55 (m, 3H), 6.48 (d, *J* = 8.5 Hz, 1H), 4.29 (td, *J*₁ = 6.7 Hz, *J*₂ = 2.6 Hz, 1H), 3.83 (s, 3H), 3.70 (dd, *J*₁ = 11.2 Hz, *J*₂ = 6.2 Hz, 1H), 3.58 (dd, *J*₁ = 10.6 Hz, *J*₂ = 8.0 Hz, 1H), 3.51 (dt, *J*₁ = 9.0 Hz, *J*₂ = 6.9 Hz, 1H), 3.44 (dd, *J*₁ = 11.2 Hz, *J*₂ = 2.6 Hz, 1H), 3.38 (dd, *J*₁ = 10.6 Hz, *J*₂ = 4.6 Hz, 1H), 3.31–3.28 (m, 1H), 3.20–3.11 (m, 1H), 2.23–2.14 (m, 1H), 2.00–1.87 (m, 1H); (¹³C NMR, 100 MHz, DMSO-*d*₆): δ = 164.1, 161.5, 157.4, 147.8, 143.4, 137.0, 129.3, 128.6, 127.3, 122.1, 113.4, 112.0, 111.8, 106.9, 62.0, 55.3, 54.9, 52.3, 50.8, 48.0, 41.7, 29.5; ESI-MS m/z calculated for $C_{25}H_{28}N_4O_2^+$ [M + 2H]⁺ 416.5; found 416.4; HRMS (ESI) for $C_{25}H_{27}N_4O_2^+$ [M + H]⁺ 415.2134; found 415.2141.

4-Methoxy-N-(4-(2-(pyridin-2-yl)-2,8-diazaspiro[4.5]decan-8-yl)phenyl)benzamide (4f). 4f was synthesized using 3e (25 mg, 0.07 mmol) in general procedure C to afford 4f (12 mg, 40% yield) as a white solid. (¹H NMR, 400 MHz, DMSO-*d*₆): δ = 9.87 (s, 1H), 8.04 (dd, *J*₁ = 5.0 Hz, *J*₂ = 1.3 Hz, 1H), 7.94 (dt, *J*₁ = 8.9 Hz, *J*₂ = 2.8 Hz, 2H), 7.59 (d, *J* = 9.1 Hz, 2H), 7.46 (ddd, *J*₁ = 9.0 Hz, *J*₂ = 7.0 Hz, *J*₃ = 2.0 Hz, 1H), 7.04 (dt, *J*₁ = 8.9 Hz, *J*₂ = 2.8 Hz, 2H), 6.94 (d, *J* = 9.1 Hz, 2H), 6.52 (dd, *J*₁ = 6.6 Hz, *J*₂ = 5.1 Hz, 1H), 6.43 (d, *J* = 8.5 Hz, 1H), 3.83 (s, 3H), 3.45 (t, *J* = 7.0 Hz, 2H), 3.31 (s, 2H), 3.24–3.19 (m, 2H), 3.13–3.07 (m, 2H), 1.88 (t, *J* = 7.0 Hz, 2H), 1.73–1.63 (m, 4H); (¹³C NMR, 100 MHz, DMSO-*d*₆): δ = 164.3, 161.6, 157.0, 147.8, 147.6, 136.8, 131.0, 129.4, 127.2, 121.5, 115.9, 113.5, 111.0, 106.2, 56.1, 55.4, 54.9, 46.6, 44.7, 35.2, 34.2, 30.7; ESI-MS m/z calculated for $C_{27}H_{31}N_4O_2^+$ [M + H]⁺ 443.6; found 443.5; HRMS (ESI) for $C_{27}H_{31}N_4O_2^+$ [M + H]⁺ 443.2447; found 443.2457.

4-Methoxy-N-(4-(9-(pyridin-2-yl)-3,9-diazaspiro[5.5]undecan-3-yl)phenyl)benzamide (4g). 4g was synthesized using 3f (120 mg, 0.32 mmol) in general procedure C to afford 4g (63 mg, 43% yield) as a white solid. (¹H NMR, 400 MHz, DMSO-*d*₆): δ = 9.86 (s, 1H), 8.09 (dd, *J*₁ = 4.8 Hz, *J*₂ = 1.7 Hz, 1H), 7.94 (d, *J* = 8.8 Hz, 2H), 7.58 (d, *J* = 9.0 Hz, 2H), 7.49 (ddd, *J*₁ = 8.7 Hz, *J*₂ = 7.0 Hz, *J*₃ = 1.9 Hz, 1H), 7.04 (d, *J* = 8.8 Hz, 2H), 6.92 (d, *J* = 9.0 Hz, 2H), 6.79 (d, *J* = 8.6 Hz, 1H), 6.57 (dd, *J*₁ = 6.9 Hz, *J*₂ = 5.0 Hz, 1H), 3.83 (s, 3H), 3.52 (t, *J* = 5.5 Hz,

4H), 3.13 (t, *J* = 5.3 Hz, 4H), 1.61 (t, *J* = 5.4 Hz, 4H), 1.51 (t, *J* = 5.6 Hz, 4H); (¹³C NMR, 100 MHz, DMSO-*d*₆): δ = 164.3, 161.6, 159.0, 147.7, 147.5, 137.3, 130.8, 129.3, 127.2, 121.5, 115.6, 113.5, 112.2, 106.8, 66.3, 59.7, 55.3, 44.5, 34.8, 34.5, 29.3; ESI-MS m/z calculated for $C_{28}H_{33}N_4O_2^+$ [M + H]⁺ 457.6; found 457.6; HRMS (ESI) for $C_{28}H_{33}N_4O_2^+$ [M + H]⁺ 457.2604; found 457.2610.

4-Methoxy-N-(4-(5-(pyridin-2-yl)-2,5-diazabicyclo[2.2.1]heptan-2-yl)phenyl)benzamide (4h). 4h was synthesized using 3g (59 mg, 0.18 mmol) in general procedure C to afford 4h (25 mg, 34% yield) as a white solid. (¹H NMR, 400 MHz, DMSO-*d*₆): δ = 9.78 (s, 1H), 8.02 (dd, *J*₁ = 5.0 Hz, *J*₂ = 1.2 Hz, 1H), 7.92 (dt, *J*₁ = 8.8 Hz, *J*₂ = 2.6 Hz, 2H), 7.51 (d, *J* = 8.9 Hz, 2H), 7.43 (ddd, *J*₁ = 8.6 Hz, *J*₂ = 7.0 Hz, *J*₃ = 1.9 Hz, 1H), 7.03 (dt, *J*₁ = 8.8 Hz, *J*₂ = 2.8 Hz, 2H), 6.57 (d, *J* = 9.0 Hz, 2H), 6.52 (dd, *J*₁ = 6.5 Hz, *J*₂ = 5.1 Hz, 1H), 6.46 (d, *J* = 8.5 Hz, 1H), 4.85 (s, 1H), 4.59 (s, 1H), 3.83 (s, 3H), 3.61 (dd, *J*₁ = 8.8 Hz, *J*₂ = 1.8 Hz, 1H), 3.51 (dd, *J*₁ = 9.5 Hz, *J*₂ = 1.5 Hz, 1H), 3.32 (d, *J* = 11.5 Hz, 2H), 2.97 (d, *J* = 8.9 Hz, 1H), 2.04 (dd, *J*₁ = 14.7 Hz, *J*₂ = 9.4 Hz, 2H); (¹³C NMR, 100 MHz, DMSO-*d*₆): δ = 164.1, 161.6, 156.8, 147.8, 143.5, 137.1, 129.3, 128.7, 127.3, 123.0, 113.5, 112.4, 111.8, 106.9, 56.8, 56.1, 55.9, 55.4, 52.4, 37.2; ESI-MS m/z calculated for $C_{24}H_{26}N_4O_2^+$ [M + 2H]⁺ 402.5; found 402.4; HRMS (ESI) for $C_{24}H_{25}N_4O_2^+$ [M + H]⁺ 401.1978; found 401.2000.

4-Methoxy-N-(4-(3-(pyridin-2-yl)-3,8-diazabicyclo[3.2.1]octan-8-yl)phenyl)benzamide (4i). 4i was synthesized using 3h (1.2 g, 3.7 mmol) in general procedure C to afford 4i (960 mg, 63% yield) as a white solid. (¹H NMR, 400 MHz, DMSO-*d*₆): δ = 9.83 (s, 1H), 8.07 (dd, *J*₁ = 4.9 Hz, *J*₂ = 1.3 Hz, 1H), 7.92 (dt, *J*₁ = 8.8 Hz, *J*₂ = 2.8 Hz, 2H), 7.58 (d, *J* = 9.0 Hz, 2H), 7.49 (ddd, *J*₁ = 8.7 Hz, *J*₂ = 7.0 Hz, *J*₃ = 2.0 Hz, 1H), 7.03 (dt, *J*₁ = 8.9 Hz, *J*₂ = 2.9 Hz, 2H), 6.92 (d, *J* = 9.1 Hz, 2H), 6.68 (d, *J* = 8.6 Hz, 1H), 6.61 (dd, *J*₁ = 6.7 Hz, *J*₂ = 5.0 Hz, 1H), 4.40 (s, 2H), 3.83 (s, 3H), 3.61 (d, *J* = 10.7 Hz, 2H), 3.11 (d, *J* = 10.7 Hz, 2H), 1.95 (t, *J* = 4.0 Hz, 2H), 1.77 (q, *J* = 5.9 Hz, 2H); (¹³C NMR, 100 MHz, DMSO-*d*₆): δ = 164.2, 161.6, 159.9, 147.4, 143.0, 137.2, 129.8, 129.3, 127.2, 122.0, 115.5, 113.5, 112.7, 106.3, 55.4, 53.9, 46.8, 27.2; ESI-MS m/z calculated for $C_{25}H_{28}N_4O_2^+$ [M + 2H]⁺ 416.5; found 416.5; HRMS (ESI) for $C_{25}H_{27}N_4O_2^+$ [M + H]⁺ 415.2134; found 415.2148.

4-Methoxy-N-(4-(3-(quinolin-3-yl)-3,8-diazabicyclo[3.2.1]octan-8-yl)phenyl)benzamide (4j). 4j was synthesized using 3h (67 mg, 0.2 mmol) and 3-bromoquinoline (83 mg, 0.4 mmol) in general procedure C to afford 4j (69 mg, 74% yield) as a yellow solid. (¹H NMR, 400 MHz, DMSO-*d*₆): δ = 9.84 (s, 1H), 8.83 (d, *J* = 2.9 Hz, 1H), 7.92 (dt, *J*₁ = 8.9 Hz, *J*₂ = 2.8 Hz, 2H), 7.85–7.81 (m, 1H), 7.74–7.71 (m, 1H), 7.59 (d, *J* = 9.0 Hz, 2H), 7.44–7.42 (m, 2H), 7.39 (d, *J* = 2.8 Hz, 1H), 7.03 (dt, *J*₁ = 8.9 Hz, *J*₂ = 2.9 Hz, 2H), 6.95 (d, *J* = 9.1 Hz, 2H), 4.46 (s, 2H), 3.82 (s, 3H), 3.56 (d, *J* = 10.0 Hz, 2H), 3.16 (d, *J* = 10.4 Hz, 2H), 2.02–1.94 (m, 4H); (¹³C NMR, 100 MHz, DMSO-*d*₆): δ = 164.2, 161.6, 144.7, 142.9, 142.5, 141.6, 129.9, 129.3, 128.6, 128.3, 127.2, 126.6, 126.5, 125.3, 122.0, 115.6, 113.7, 113.5, 55.4, 54.9, 54.1, 49.2, 27.3; ESI-MS m/z calculated for $C_{29}H_{30}N_4O_2^+$ [M + 2H]⁺ 466.6; found 466.3; HRMS (ESI) for $C_{29}H_{29}N_4O_2^+$ [M + H]⁺ 465.2291; found 465.2300.

4-Methoxy-N-(4-(3-(quinoxalin-2-yl)-3,8-diazabicyclo[3.2.1]octan-8-yl)phenyl)benzamide (4k). To a solution of 3h (50 mg, 0.15 mmol) in 1.5 mL of DMF, 2-bromoquinoline (62 mg, 0.3 mmol) and DIPEA (65 μL, 0.38 mmol) were added. The reaction mixture was heated at 100 °C for 16 h and cooled to RT. The mixture was diluted with CH₂Cl₂ and washed using aq saturated NaHCO₃ solution. The organic layer was separated, dried over Na₂SO₄, filtered, and concentrated *in vacuo*. The crude product was purified by flash chromatography on silica gel (CH₂Cl₂/7 N NH₃ in MeOH = 40:1) to afford 4k (36 mg, 52%) as a yellow solid. (¹H NMR, 400 MHz, DMSO-*d*₆): δ = 9.85 (s, 1H), 8.73 (s, 1H), 7.92 (d, *J* = 2.8 Hz, 2H), 7.81 (d, *J* = 8.0 Hz, 1H), 7.62–7.58 (m, 4H), 7.40–7.36 (m, 1H), 7.03 (dt, *J*₁ = 8.9 Hz, *J*₂ = 2.8 Hz, 2H), 6.97 (d, *J* = 9.0 Hz, 2H), 4.47 (s, 2H), 4.12 (d, *J* = 11.7 Hz, 2H), 3.82 (s, 3H), 3.36 (d, *J* = 11.5 Hz, 2H), 1.98 (t, *J* = 4.2 Hz, 2H), 1.82 (q, *J* = 5.9 Hz, 2H); (¹³C NMR, 100 MHz, DMSO-*d*₆): δ = 164.2, 161.6, 153.1, 142.8, 141.0, 136.4, 136.3, 130.0, 129.9, 129.3, 128.3, 127.2, 125.9, 124.2, 122.1, 122.0, 115.6, 113.5, 55.3, 54.9, 53.9, 46.3, 26.9; ESI-MS m/z calculated for $C_{28}H_{29}N_5O_2^+$ [M + 2H]⁺ 467.6; found 467.5; HRMS (ESI) for $C_{28}H_{28}N_5O_2^+$ [M + H]⁺ 466.2243; found 466.2240.

4-Methoxy-N-(4-(3-(pyridin-2-yl)-3,9-diazabicyclo[3.3.1]nonan-9-yl)phenyl)benzamide (4l). **4l** was synthesized using **3i** (28 mg, 0.08 mmol) in general procedure C to afford **4l** (7 mg, 19% yield) as a white solid. (¹H NMR, 400 MHz, DMSO-*d*₆): δ = 9.88 (s, 1H), 8.13 (dd, *J*₁ = 4.9 Hz, *J*₂ = 1.4 Hz, 1H), 7.95 (dt, *J*₁ = 8.9 Hz, *J*₂ = 2.8 Hz, 2H), 7.61 (d, *J* = 9.0 Hz, 2H), 7.54 (ddd, *J*₁ = 8.7 Hz, *J*₂ = 6.9 Hz, *J*₃ = 2.0 Hz, 1H), 7.05 (dt, *J*₁ = 8.9 Hz, *J*₂ = 2.8 Hz, 2H), 6.93 (d, *J* = 9.1 Hz, 2H), 6.87 (d, *J* = 8.7 Hz, 1H), 6.58 (dd, *J*₁ = 6.9 Hz, *J*₂ = 5.0 Hz, 1H), 4.64 (s, 2H), 3.84 (s, 3H), 3.77 (d, *J* = 11.0 Hz, 2H), 2.97 (dd, *J*₁ = 11.4 Hz, *J*₂ = 3.2 Hz, 2H), 2.48–2.42 (m, 1H), 1.80 (d, *J* = 6.2 Hz, 4H), 1.50–1.47 (m, 1H); (¹³C NMR, 100 MHz, DMSO-*d*₆): δ = 164.2, 161.6, 157.4, 147.9, 146.8, 137.6, 130.6, 129.4, 127.2, 121.6, 114.4, 113.5, 112.1, 107.0, 55.4, 51.9, 46.5, 27.8, 19.8; ESI-MS *m/z* calculated for C₂₆H₃₀N₄O₂⁺ [M + 2H]⁺ 430.6; found 430.5; HRMS (ESI) for C₂₆H₂₉N₄O₂⁺ [M + H]⁺ 429.2291; found 429.2291.

4-Methoxy-N-(4-(4-(pyridin-2-yl)-1,4-diazepan-1-yl)phenyl)benzamide (4m). **4m** was synthesized using **3j** (65 mg, 0.15 mmol) in general procedure C to afford **4m** (24 mg, 40% yield) as a white solid. (¹H NMR, 400 MHz, DMSO-*d*₆): δ = 9.77 (s, 1H), 8.05 (dd, *J*₁ = 4.9 Hz, *J*₂ = 1.4 Hz, 1H), 7.92 (dt, *J*₁ = 8.8 Hz, *J*₂ = 2.8 Hz, 2H), 7.52 (d, *J* = 9.0 Hz, 2H), 7.46 (ddd, *J*₁ = 8.7 Hz, *J*₂ = 6.9 Hz, *J*₃ = 2.0 Hz, 1H), 7.03 (dt, *J*₁ = 8.9 Hz, *J*₂ = 2.9 Hz, 2H), 6.73 (d, *J* = 9.1 Hz, 2H), 6.66 (d, *J* = 8.6 Hz, 1H), 6.51 (dd, *J*₁ = 6.9 Hz, *J*₂ = 5.1 Hz, 1H), 3.83 (s, 3H), 3.81 (t, *J* = 5.7 Hz, 2H), 3.59 (t, *J* = 5.2 Hz, 2H), 3.48 (t, *J* = 6.0 Hz, 2H), 3.40 (t, *J* = 5.9 Hz, 2H), 2.00–1.94 (m, 2H); (¹³C NMR, 100 MHz, DMSO-*d*₆): δ = 164.1, 161.5, 157.1, 147.8, 143.8, 137.4, 129.3, 128.2, 127.3, 122.3, 113.5, 111.3₄, 111.2₈, 105.6, 55.4, 48.8, 47.2, 46.1, 45.6, 23.8; ESI-MS *m/z* calculated for C₂₄H₂₈N₄O₂⁺ [M + 2H]⁺ 404.5; found 404.5; HRMS (ESI) for C₂₄H₂₇N₄O₂⁺ [M + H]⁺ 403.2134; found 403.2117.

N-(4-(4-(5-Chloropyridin-2-yl)piperazin-1-yl)phenyl)-4-methoxybenzamide (4n). **4n** was synthesized using **1a** (48 mg, 0.14 mmol) and 1-(5-chloropyridin-2-yl)piperazine (20 mg, 34% yield) in general procedure A to afford **4n** (20 mg, 34% yield) as a white solid. (¹H NMR, 400 MHz, DMSO-*d*₆): δ = 9.91 (s, 1H), 8.14 (d, *J* = 2.7 Hz, 1H), 7.94 (dt, *J*₁ = 8.9 Hz, *J*₂ = 2.8 Hz, 2H), 7.62 (dd, *J*₁ = 9.1 Hz, *J*₂ = 2.4 Hz, 3H), 7.04 (dt, *J*₁ = 8.9 Hz, *J*₂ = 2.8 Hz, 2H), 6.98 (d, *J* = 9.1 Hz, 2H), 6.95 (d, *J* = 9.2 Hz, 1H), 3.83 (s, 3H), 3.63 (t, *J* = 4.8 Hz, 4H), 3.19 (t, *J* = 5.1 Hz, 4H); (¹³C NMR, 100 MHz, DMSO-*d*₆): δ = 164.3, 161.7, 157.5, 147.2, 145.6, 137.2, 131.6, 129.4, 127.1, 121.4, 119.0, 116.0, 113.5, 108.6, 55.4, 48.5, 44.7; ESI-MS *m/z* calculated for C₂₃H₂₄ClN₄O₂⁺ [M + H]⁺ 423.9; found 423.4; HRMS (ESI) for C₂₃H₂₄ClN₄O₂⁺ [M + H]⁺ 423.1588; found 423.1598.

4-Methoxy-N-(5-(4-(pyridin-2-yl)piperazin-1-yl)pyridin-2-yl)benzamide (4o). **4o** was synthesized using **3k** (54 mg, 0.17 mmol) in general procedure C to afford **4o** (42 mg, 63% yield) as a white solid. (¹H NMR, 400 MHz, DMSO-*d*₆): δ = 10.41 (s, 1H), 8.15–8.12 (m, 2H), 8.05–8.02 (m, 3H), 7.56 (ddd, *J*₁ = 8.7 Hz, *J*₂ = 7.0 Hz, *J*₃ = 2.0 Hz, 1H), 7.51 (dd, *J*₁ = 9.1 Hz, *J*₂ = 3.0 Hz, 1H), 7.02 (d, *J* = 8.8 Hz, 2H), 6.91 (d, *J* = 8.6 Hz, 1H), 6.67 (dd, *J*₁ = 7.0 Hz, *J*₂ = 5.0 Hz, 1H), 3.83 (s, 3H), 3.65 (t, *J* = 4.8 Hz, 4H), 3.26 (t, *J* = 5.1 Hz, 4H); (¹³C NMR, 100 MHz, DMSO-*d*₆): δ = 174.3, 171.6, 168.6, 157.2, 154.5, 153.4, 147.2, 145.0, 139.4, 136.0, 134.8, 124.8, 123.2, 122.9, 117.0, 65.0, 57.8, 54.1; ESI-MS *m/z* calculated for C₂₂H₂₄N₅O₂⁺ [M + H]⁺ 390.5; found 390.4; HRMS (ESI) for C₂₂H₂₄N₅O₂⁺ [M + H]⁺ 390.1930; found 390.1929.

4-Methoxy-N-(5-(3-(pyridin-2-yl)-3,8-diazabicyclo[3.2.1]octan-8-yl)pyridin-2-yl)benzamide (4p). **4p** was synthesized using **3l** (80 mg, 0.18 mmol) in general procedure C to afford **4p** (17 mg, 23% yield) as a yellow oil. (¹H NMR, 400 MHz, MeOD): δ = 8.05 (dd, *J*₁ = 4.9 Hz, *J*₂ = 1.3 Hz, 2H), 7.98 (d, *J* = 8.9 Hz, 1H), 7.93 (d, *J* = 8.8 Hz, 2H), 7.53 (ddd, *J*₁ = 8.7 Hz, *J*₂ = 7.0 Hz, *J*₃ = 1.9 Hz, 1H), 7.46 (dd, *J*₁ = 9.1 Hz, *J*₂ = 2.4 Hz, 1H), 7.03 (d, *J* = 8.8 Hz, 2H), 6.72 (d, *J* = 8.7 Hz, 1H), 6.66 (dd, *J*₁ = 6.9 Hz, *J*₂ = 5.2 Hz, 1H), 4.44 (brs, 2H), 3.86 (s, 3H), 3.80 (dd, *J*₁ = 12.2 Hz, *J*₂ = 1.4 Hz, 2H), 3.21 (d, *J* = 11.6 Hz, 2H), 2.06 (t, *J* = 4.0 Hz, 2H), 1.91 (d, *J* = 5.8 Hz, 2H); (¹³C NMR, 100 MHz, DMSO-*d*₆): δ = 167.8, 164.5, 161.7, 158.3, 148.2, 144.3, 139.3, 136.7, 130.7, 126.8, 114.5, 109.4, 108.6, 56.3, 56.1, 28.5; ESI-MS *m/z* calculated for C₂₄H₂₆N₅O₂⁺ [M + H]⁺ 416.5; found 416.4; HRMS (ESI) for C₂₄H₂₆N₅O₂⁺ [M + H]⁺ 416.2087; found 416.2087.

4-Methoxy-N-(5-(4-(pyridin-2-yl)-1,4-diazepan-1-yl)pyridin-2-yl)benzamide (4q). **4q** was synthesized using **3m** (71 mg, 0.22 mmol) in general procedure C to afford **4q** (60 mg, 68% yield) as a white solid. (¹H NMR, 400 MHz, MeOD): δ = 8.00 (d, *J* = 4.4 Hz, 1H), 7.92 (d, *J* = 8.7 Hz, 2H), 7.86 (d, *J* = 9.0 Hz, 2H), 7.47 (ddd, *J*₁ = 8.9 Hz, *J*₂ = 6.7 Hz, *J*₃ = 1.4 Hz, 1H), 7.26 (dd, *J*₁ = 9.1 Hz, *J*₂ = 2.9 Hz, 1H), 7.02 (d, *J* = 8.7 Hz, 2H), 6.68 (d, *J* = 8.7 Hz, 1H), 6.54 (t, *J* = 5.9 Hz, 1H), 3.88 (t, *J* = 4.9 Hz, 5H), 3.69 (t, *J* = 5.5 Hz, 2H), 3.57 (t, *J* = 6.0 Hz, 2H), 3.51 (t, *J* = 6.0 Hz, 2H), 2.09–2.03 (m, 2H); (¹³C NMR, 100 MHz, MeOD): δ = 167.8, 164.4, 158.8, 148.5, 143.0, 142.5, 139.4, 132.3, 130.6, 122.4, 118.3, 115.0, 113.1, 107.8, 56.1, 55.0, 47.9, 47.7, 25.0; ESI-MS *m/z* calculated for C₂₃H₂₆N₅O₂⁺ [M + H]⁺ 404.5; found 404.4; HRMS (ESI) for C₂₃H₂₆N₅O₂⁺ [M + H]⁺ 404.2087; found 404.2084.

4-Methoxy-N-(6-(3-(pyridin-2-yl)-3,8-diazabicyclo[3.2.1]octan-8-yl)pyridin-3-yl)benzamide (4r). **4r** was synthesized using **3n** (510 mg, 0.15 mmol) in general procedure C to afford **4r** (83 mg, 13% yield) as a white solid. (¹H NMR, 400 MHz, DMSO-*d*₆): δ = 9.95 (s, 1H), 8.45 (d, *J* = 2.6 Hz, 1H), 8.08 (dd, *J*₁ = 4.8 Hz, *J*₂ = 1.4 Hz, 1H), 7.94 (dt, *J*₁ = 8.8 Hz, *J*₂ = 2.9 Hz, 2H), 7.90 (dd, *J*₁ = 9.0 Hz, *J*₂ = 2.6 Hz, 1H), 7.49 (ddd, *J*₁ = 8.7 Hz, *J*₂ = 7.0 Hz, *J*₃ = 2.0 Hz, 1H), 7.05 (dt, *J*₁ = 8.9 Hz, *J*₂ = 2.9 Hz, 2H), 6.91 (d, *J* = 9.0 Hz, 1H), 6.70 (d, *J* = 8.6 Hz, 1H), 6.61 (dd, *J*₁ = 6.7 Hz, *J*₂ = 5.0 Hz, 1H), 4.67 (s, 2H), 3.88 (dd, *J*₁ = 12.2 Hz, *J*₂ = 1.8 Hz, 2H), 3.83 (s, 3H), 3.05 (dd, *J*₁ = 11.9 Hz, *J*₂ = 1.5 Hz, 2H), 1.92 (t, *J* = 4.0 Hz, 2H), 1.77 (q, *J* = 5.7 Hz, 2H); (¹³C NMR, 100 MHz, DMSO-*d*₆): δ = 164.6, 161.8, 159.8, 154.0, 147.4, 140.8, 137.2, 131.3, 129.4, 126.7₁, 126.6₅, 113.5, 112.7, 108.7, 106.4, 55.4, 55.2, 48.0, 27.1; ESI-MS *m/z* calculated for C₂₄H₂₇N₅O₂⁺ [M + 2H]⁺ 417.5; found 417.5; HRMS (ESI) for C₂₄H₂₆N₅O₂⁺ [M + H]⁺ 416.2087; found 416.2087.

4-Methoxy-N-(4-(4-methylpiperazin-1-yl)phenyl)benzamide (5a). **5a** was synthesized using **1a** (177 mg, 0.5 mmol) and 1-methylpiperazine (55 μL, 0.5 mmol) in general procedure A to afford **5a** (57 mg, 35% yield) as a white solid. (¹H NMR, 400 MHz, MeOD): δ = 7.89 (dt, *J*₁ = 8.8 Hz, *J*₂ = 2.8 Hz, 2H), 7.53 (d, *J* = 9.0 Hz, 2H), 7.02 (dt, *J*₁ = 8.8 Hz, *J*₂ = 2.9 Hz, 2H), 6.98 (dt, *J*₁ = 9.0 Hz, *J*₂ = 3.2 Hz, 2H), 3.86 (s, 3H), 3.19 (t, *J* = 4.8 Hz, 4H), 2.63 (t, *J* = 5.0 Hz, 4H), 2.35 (s, 3H); (¹³C NMR, 100 MHz, MeOD): δ = 164.2, 149.8, 132.8, 132.4, 130.6, 128.4, 123.8, 117.9, 114.9, 56.1₄, 56.0₉, 50.5, 46.2; ESI-MS *m/z* calculated for C₁₉H₂₅N₃O₂⁺ [M + 2H]⁺ 327.4; found 327.4; HRMS (ESI) for C₁₉H₂₄N₃O₂⁺ [M + H]⁺ 326.1869; found 326.1855.

N-(4-(1-Azaspiro[3.5]nonan-1-yl)phenyl)-4-methoxybenzamide (5b). **5b** was synthesized using **1a** (85 mg, 0.24 mmol) and 1-azaspiro[3.5]nonane (33 mg, 0.26 mmol) in general procedure A to afford **5b** (9 mg, 11% yield) as a white waxy solid. (¹H NMR, 400 MHz, MeOD): δ = 7.88 (dt, *J*₁ = 8.8 Hz, *J*₂ = 2.8 Hz, 2H), 7.40 (d, *J* = 8.8 Hz, 2H), 7.01 (dt, *J*₁ = 8.9 Hz, *J*₂ = 2.9 Hz, 2H), 6.56 (dt, *J*₁ = 8.9 Hz, *J*₂ = 3.0 Hz, 2H), 3.86 (s, 3H), 3.65 (t, *J* = 7.2 Hz, 2H), 2.10 (t, *J* = 7.2 Hz, 2H), 1.92 (td, *J*₁ = 12.8 Hz, *J*₂ = 1.7 Hz, 2H), 1.80–1.71 (m, 4H), 1.41–1.28 (m, 3H), 1.20 (tt, *J*₁ = 12.0 Hz, *J*₂ = 4.1 Hz, 1H); (¹³C NMR, 100 MHz, MeOD): δ = 164.1, 147.5, 130.5, 130.4, 128.5, 124.1, 115.1, 114.9, 72.2, 56.1, 46.5, 36.6, 29.6, 26.8, 24.4; ESI-MS *m/z* calculated for C₂₂H₂₈N₂O₂⁺ [M + 2H]⁺ 352.5; found 352.5; HRMS (ESI) for C₂₂H₂₇N₂O₂⁺ [M + H]⁺ 351.2073; found 351.2086.

4-Methoxy-N-(4-(3-methoxyazetidide-1-yl)phenyl)benzamide (5c). **5c** was synthesized using **1a** (200 mg, 0.56 mmol) and 3-methoxyazetidide (77 mg, 0.62 mmol) in general procedure A to afford **5c** (85 mg, 49% yield) as a white solid. (¹H NMR, 400 MHz, DMSO-*d*₆): δ = 9.83 (s, 1H), 7.93 (dt, *J*₁ = 8.8 Hz, *J*₂ = 2.8 Hz, 2H), 7.54 (d, *J* = 8.8 Hz, 2H), 7.04 (dt, *J*₁ = 8.9 Hz, *J*₂ = 2.8 Hz, 2H), 6.44 (dt, *J*₁ = 8.8 Hz, *J*₂ = 2.9 Hz, 2H), 4.33–4.28 (m, 1H), 4.03 (t, *J* = 7.5 Hz, 2H), 3.83 (s, 3H), 3.55 (dd, *J*₁ = 8.2 Hz, *J*₂ = 4.5 Hz, 2H), 3.24 (s, 3H); (¹³C NMR, 100 MHz, DMSO-*d*₆): δ = 164.2, 161.6, 148.2, 129.8, 129.3, 127.2, 121.8, 113.5, 111.4, 69.3, 58.8, 55.4, 55.4; ESI-MS *m/z* calculated for C₁₈H₂₂N₂O₃⁺ [M + 2H]⁺ 314.4; found 314.4; HRMS (ESI) for C₁₈H₂₁N₂O₃⁺ [M + H]⁺ 313.1552; found 313.1566.

4-Hydroxy-N-(4-(3-(pyridin-2-yl)-3,8-diazabicyclo[3.2.1]octan-8-yl)phenyl)benzamide (6). To a solution of **4i** (214 mg, 0.53 mmol) in 5.3 mL of CH₂Cl₂, BBr₃ (152 μL, 1.6 mmol) was slowly added. The reaction mixture was stirred at RT for 24 h. After the completion of the reaction, the mixture was diluted with CH₂Cl₂. The organic layer was washed with aq saturated NaHCO₃ and brine, dried over Na₂SO₄, and

filtered. The volatiles were removed under reduced pressure, and the crude product was purified by flash chromatography on silica gel ($\text{CH}_2\text{Cl}_2/7\text{ N NH}_3$ in $\text{MeOH} = 20:1$) to afford **5** (85 mg, 40% yield) as a white solid. ($^1\text{H NMR}$, 400 MHz, $\text{DMSO}-d_6$): $\delta = 10.01$ (s, 1H), 9.73 (s, 1H), 8.07 (s, 1H), 7.81 (d, $J = 8.0$ Hz, 2H), 7.55 (d, $J = 8.0$ Hz, 2H), 7.49 (t, $J = 7.6$ Hz, 1H), 6.91 (d, $J = 8.1$ Hz, 2H), 6.83 (d, $J = 8.1$ Hz, 2H), 6.68 (d, $J = 8.4$ Hz, 1H), 6.61 (brs, 1H), 4.39 (s, 2H), 3.75 (d, $J = 12.0$ Hz, 2H), 3.10 (d, $J = 12.0$ Hz, 2H), 1.94 (brs, 2H), 1.77 (d, $J = 6.7$ Hz, 2H); ($^{13}\text{C NMR}$, 100 MHz, $\text{DMSO}-d_6$): $\delta = 164.9, 160.7, 160.4, 147.9, 143.4, 137.7, 130.4, 129.9, 126.2, 122.5, 116.0, 115.3, 113.2, 106.8, 54.4, 47.3, 27.7$; ESI-MS m/z calculated for $\text{C}_{24}\text{H}_{26}\text{N}_4\text{O}_2^+ [\text{M} + 2\text{H}]^+$ 402.5; found 402.6; HRMS (ESI) for $\text{C}_{24}\text{H}_{25}\text{N}_4\text{O}_2^+ [\text{M} + \text{H}]^+$ 401.1978; found 401.1993.

In Vitro Radioligand Binding Competition Assay. α -Syn Assay Using [^3H]BF2846. Three concentrations of tested compounds (10 nM, 100 nM, and 1 μM) and [^3H]BF2846 (~ 4 nM) were added to 50 nM of recombinant α -syn fibrils in a working buffer (50 mM Tris-HCl, 0.01% bovine serum albumin (BSA)). The mixture (150 μL) was gently mixed by agitation, covered, and then incubated at 37 $^\circ\text{C}$ for 1.5 h in a nonbinding 96 well plate (Corning, 3605). The mixture was filtered through a Unifilter-96 harvesting system (PerkinElmer) and then washed three times with 250 μL of ice-cold buffer containing 10 mM Tris-HCl (pH 7.4), 15 mM NaCl, and 20% EtOH. 50 μL of scintillation cocktail (MicroScint-20, PerkinElmer) was added to the collected filtrate and counted on a Microbeta system (PerkinElmer). Total binding was measured in the absence of tested compounds, and nonspecific binding was defined by the presence of 100 nM unlabeled BF2846 in the working buffer. The data analysis was carried out in the following equations and graphically presented with a heatmap.

$$\text{Percentage inhibition (\%)} = \left(1 - \frac{\text{Competitor Binding Counts} - \text{Nonspecific Binding Counts}}{\text{Total Binding Counts} - \text{Nonspecific Binding Counts}} \right) \times 100$$

For the full curve of α -syn binding affinity, [^3H]BF2846 (~ 4 nM) was incubated with fixed concentrations of 50 nM α -syn fibrils and ten concentrations of tested compounds (0.05–1000 nM). All data points were collected in three individual experiments. The equilibrium dissociation constants, K_i values, were obtained from EC_{50} using the equation $K_i = \text{EC}_{50} / (1 + [\text{radioligand}] / K_D)$ by nonlinear regression from GraphPad Prism v.9.3.1.

$\text{A}\beta$ Assay Using [^3H]PiB. Three concentrations of tested compounds (10 nM, 100 nM, and 1 μM), [^3H]PiB (~ 32 nM), and 0.5 $\mu\text{g}/\mu\text{L}$ of AD, CAA- tissue homogenate (Tissue ID: 05-215) in Dulbecco's phosphate-buffered saline (DPBS) were added to each well of a nonbinding 96 well plate. Nonspecific binding was defined by 1 μM of unlabeled PiB in DPBS. The following procedures were performed in the same procedure as the α -syn assay using DPBS instead of the working buffer.

Post-mortem PSP and CBD Tissues. The binding assays utilized fresh frozen, autopsy-confirmed, post-mortem human PSP and CBD brain tissue blocks (1 cm^3) obtained from the Neurodegenerative Disease Brain Bank at the University of California, San Francisco, containing only frequent 4R-tau aggregates (PSP tissue, superior frontal gyrus, or CBD tissue, middle frontal gyrus) and no other detectable aggregated amyloid or TDP-43 species. The frozen tissue blocks were separately thawed and homogenized in ice-cold, pH 7.0 PBS at 300 mg/mL on ice using a glass homogenizer, diluted 30-fold with PBS to 10 mg/mL, and homogenized a second time with a Brinkmann Polytron homogenizer before storage at -80 $^\circ\text{C}$. At the time of the binding assays, frozen brain tissue homogenates were thawed to RT and diluted 10-fold in PBS to a concentration of 1 mg/mL.

In Vitro Competition (K_i) Assays of **4i vs Tritiated Tau Radioligands.** The equilibrium inhibition constant (K_i) values of unlabeled **4i** were determined versus tritiated tau radioligands using published methods.⁵⁶ Briefly, the concentration of **4i** (~ 400 μM in the stock solution) was determined by quantitative NMR in $\text{DMSO}-d_6$ (0.25% DMSO in the final assay vials). The appropriate concentrations (ranging from 0.1 to 1000 nM) of **4i** in 400 μL of Tris buffer (pH 7.0)

were combined with 500 μL of tritiated radioligand in Tris buffer (~ 1 nM final concentration of radioligand). The assay was initiated by the addition of 100 μL of 1 mg/mL brain tissue homogenate to achieve a final concentration of 100 μg tissue/mL. After incubation for 60 min at 37 $^\circ\text{C}$ with shaking, the binding mixture was filtered through a Whatman GF/B glass filter via a Brandel M-24R cell harvester (Gaithersburg, MD, USA) and rapidly washed four times with 3 mL of Tris buffer. The filters were counted in Cytoscint-ES after thorough vortexing using a liquid scintillation counter. Complete (100%) inhibition of specific binding was defined as the number of counts displaced by 1 μM of the unlabeled radioligand. All assays were performed in triplicate at each concentration.

In Vitro Saturation Assays of [^3H]4i for Various Neurodegenerative Post-mortem Brain Tissues. To 400 nM of recombinant α -syn fibrils or 50 μg /well of a panel of post-mortem brain samples (e.g., PD, MSA, or AD) in PBS or Tris buffer was added ten concentrations of [^3H]4i (1.56-fold dilution, 0.5 to 40 nM), and the total volume was 150 μL . The total binding and nonspecific binding are defined by the absence of and the presence of 1 μM of unlabeled **4i**, respectively. The following procedures were performed as in the α -syn assay. The equilibrium dissociation constant, K_D , and maximal specific binding, B_{max} are determined by fitting the data into the equation $Y = B_{\text{max}} \times X / (X + K_D)$ via nonlinear regression from GraphPad Prism v.9.3.1.

K_D in PSP and CBD tissue homogenates were measured according to a previously described method with minor modifications.⁵⁷ **4i** was dissolved in DMSO at 400 μM and then diluted to 20 μM with PBS to yield 5% DMSO/PBS. The remaining serial dilutions (typically from 6 μM to 4 nM) were made with 5% DMSO/PBS to maintain a constant DMSO concentration in the final assay tubes. 50 μL of these solutions were combined with same volume of [^3H]4i and 800 μL of Tris buffer (pH 7.0) to yield 0.25% DMSO, ~ 1 nM [^3H]4i, and 0.2 to 1000 nM of **4i** in the final assay. The assay began by addition of 100 μL of the 1 mg/mL brain homogenate to achieve a final concentration of 100 μg tissue/mL. After incubation for 60 min at 37 $^\circ\text{C}$ with shaking, the binding mixture was filtered through a Whatman GF/B glass filter via a Brandel M-24R cell harvester (Gaithersburg, MD) and rapidly washed three times with 3 mL of Tris buffer. The filters were counted in Cytoscint-ES after thorough vortexing and sitting overnight. All assays were performed at least in triplicate. The concentration of bound compound was determined from the radioactivity retained on the filter after correcting for the nondisplaceable radioactivity (defined as that remaining with ~ 1 μM of **4i**) and the specific activity of [^3H]4i after dilution with varying concentrations of **4i**. The K_D value was determined by the slope (slope = $-1/K_D$) of a Scatchard plot of the bound/free vs bound radioligand values at the different ligand concentrations, and the B_{max} value was determined by the x -axis intercept of the bound/free vs bound line.

Nuclear Emulsion Autoradiography. Frozen post-mortem PD and MSA brain tissue samples were sectioned on a cryostat at 16 μm and mounted onto glass slides and stored at -80 $^\circ\text{C}$. To quench lipofuscin autofluorescence, slides were incubated in 1 \times TrueBlack (Biotium) in 70% EtOH. Slides were incubated sequentially with antiphospho- α -syn (S129) antibody (p-syn/81A, BioLegend) and Alexa Fluor 488 goat antimouse secondary antibody to immunostain LBs and LNs. Slides were then incubated in 15 nM [^3H]4i diluted in 30 mM Tris-HCl, pH 7.4, for 2 h at 37 $^\circ\text{C}$. The slides were washed in 30 mM Tris-HCl, pH 7.4, for 1 min, 50% ethanol/30 mM Tris-HCl, pH 7.4, for 1 min, 30% ethanol/30 mM Tris-HCl, pH 7.4, for 1 min, 30 mM Tris-HCl, pH 7.4, for 1 min, and MQH₂O for 1 s. The slides were allowed to completely air-dry in a fume hood. To obtain high resolution autoradiographic information, the slides were dipped in autoradiography emulsion (Carestream Type NTB) and incubated in the dark for 4 days. The slides were developed in Ilford Phenisol Developer for 4 min, 200 mL of 1% acetic acid for 2 min, 200 mL of 1:4 Ilford Hypam Fixer for 4 min, and 200 mL of MQH₂O for 4 min (2 \times). The slides were allowed to completely air-dry in the fume hood before a coverslip was applied with Fluoromount-G Mounting Medium. Photomicrographs of fluorescent antibody staining and tritium activated silver grains were obtained on a Nikon Eclipse TE2000-U Inverted Fluorescence Microscope (Nikon,

Tokyo, Japan) using fluorescence and brightfield/monochrome light, respectively.

In Vitro Real-Time Autoradiography. For [^3H]4i autoradiography, fresh frozen brains derived from PD and MSA cases were sliced in 10- μm -thick sections, mounted on Super Frost Plus slides, and stored at $-80\text{ }^\circ\text{C}$ until further processing. Sections were allowed to thaw for 30 min at RT and then preincubated with PBS + 0.1% BSA buffer, pH 7.5, for 15 min under constant gentle shaking. Sections were then incubated for 90 min using the same buffer containing 5 nM [^3H]4i. Nonspecific binding was determined via coincubation with 1 μM 4i. Following incubation, slides were washed 2×5 min in ice-cold ($4\text{ }^\circ\text{C}$) PBS + 20% EtOH and 1×1 min in ice-cold dH_2O and then dried with a hot plate. Images were obtained by using the BeQuant, a new generation of gas detector for real time autoradiography. Briefly, a strip of copper adhesive tape was placed on the back of each microscope slide. A compressed air gun from the preparation station was applied to each sample to remove dust from the entire surface of the glass slide. Afterward, the samples were placed in the sample holder in a way that the samples must face the worktop, and the copper adhesive tape must point upward. The sample holder was covered with a compression plate and loaded in the BeQuant, and the gas injection was allowed to start. The image acquisition was performed for 1 h using the acquisition software called Bevacq. Regions of interest (ROIs) were determined manually for each section on the scanned images using Beamage software. The signal on the scanned images was given as average counts per pixel expressed as count per min per mm^2 (cp/mim/ mm^2). Based on these measurements, specific binding values were calculated in the presence of 4i (total binding – nonspecific binding).

Immunohistochemistry. Immunohistochemistry was performed on fresh frozen sections adjacent to those used for autoradiography. Sections were fixed in ethanol for 15 min, washed 3×5 min in PBS Tween-20 buffer, permeabilized with 0.1% Triton X-100 for 10 min followed by 3×5 min washes in PBST. Sections were then blocked with PBS + 10% goat serum + 1% BSA + 0.1% Tween 20 for 1 h at RT, followed by the appropriate primary antibody (Table S2), S129 antibody (P-syn/81A), antitbeta amyloid (DE2B4) antibody, or antiphospho-tau (Ser202, Thr205) antibody, details in the Table 1, used at 1:500 dilution for 16 h at $4\text{ }^\circ\text{C}$. After a series of thorough washes with PBS Tween 20 buffer, the slides were incubated with the secondary antibodies, Alexa Fluor 568, Alexa Fluor 488, or Alexa Fluor 647, details in Table 2, at 1:1000 dilution for 1 h at RT. The sections were then washed again with PBS Tween 20, 3×5 min, mounted with Duolink *in situ* mounting media with DAPI and coverslips for microscopy. Images were captured with a Zeiss microscope at $10\times$ magnification.

Radiochemistry. Radiosynthesis of [^{11}C]4i was performed in a Synthra MeIplus module with [^{11}C] CH_3I that was prepared via the gas-phase method. [^{11}C] CO_2 was produced by $^{14}\text{N}(\text{p},\alpha)^{11}\text{C}$ nuclear reaction, reduced to [^{11}C] CH_4 using Ni catalyst and, then, converted to [^{11}C] CH_3I through an iodine column. The prepared [^{11}C] CH_3I was bubbled at $-30\text{ }^\circ\text{C}$ to a mixture of 5 (1 mg, 2.5 μmol) and 1.5 μL of 5 N NaOH (3 equiv) in 0.5 mL of DMF, which had been vigorously mixed for 1 min. The mixture was heated at $70\text{ }^\circ\text{C}$ for 5 min and quenched at RT with 1 mL of HPLC mobile phase. The crude product was purified by preparative HPLC (column: Phenomenex Luna 5 μm C18 100 \AA , 10×250 mm; eluent: MeCN/10 mM NH_4HCO_3 (60:40); wavelength: 254 nm; flow rate: 4.5 mL/min; Rt: 10 min).

For microPET studies in NHP, purified [^{11}C]4i was formulated. The collected fraction from HPLC was mixed with a prefilled 50 mL of water and the mixture was passed on a 7 cm^3 tC18 cartridge. The trapped [^{11}C]4i was washed with 10 mL of water, eluted by 1 mL of EtOH, and diluted with 9 mL of normal saline. The prepared [^{11}C]4i solution was filtered through a Millex-GV filter (0.22 μm) for the injection. Radioactivity in the final product vial was measured using a dose calibrator (Capintec).

Radiochemical purity and the molar activity were determined by analytical HPLC prior to the PET study (column: Waters acquity UHPLC BEH C18 1.7 μm C18 130 \AA , 2.1×50 mm; eluent: MeCN/0.1% TFA in water (73:27); wavelength: 254 nm; flow rate: 0.5 mL/min; Rt: 1.3 min).

Partition Coefficient ($\text{LogD}_{7.4}$). Shake-flask method was used to determine $\text{LogD}_{7.4}$ of [^{11}C]4i using 5 mL of *n*-octanol and 10 mL of 0.01 M, pH 7.4 phosphate buffer solution. Ten μL of [^{11}C]4i was added to the *n*-octanol/0.01 M, pH 7.4 phosphate buffer solution, and the mixture was vigorously mixed for 1 min and placed for 20 min to be separated. Five aliquots (1 mL) of each phase were collected and counted using a Wizard² 2480 gamma counter (PerkinElmer). $\text{LogD}_{7.4}$ was expressed as the log value of the partition ratio between the two phases and averaged over 5 replicates (mean \pm SD).

PET Studies of [^{11}C]4i in Nonhuman Primates. Dynamic whole body PET of [^{11}C]4i was conducted on a 25 ± 2 year old adult male rhesus macaque using the PennPET Explorer scanner. The monkey, fasted for 12 h prior to the PET study, was initially anesthetized by intramuscular injection with ketamine (4 mg/kg) and dexmedetomidine (0.05 mg/kg). The monkey was intubated, and anesthesia was maintained with 0.75–2% isoflurane/oxygen. A percutaneous catheter was placed for the tracer injection. A low dose CT scan was performed to confirm positioning and attenuation correction followed by 90 min dynamic PET images (12×10 s, 2×30 s, 4×60 s, 2×120 s, 3×180 s, 2×300 s, 2×600 s, and 2×1200 s) acquired in list mode after venous injection of 104 ± 5 MBq of [^{11}C]4i. The PET image was reconstructed using a time-of-flight list-mode ordered subsets expectation maximization (OSEM, 25 subsets) reconstruction algorithm.⁵⁸ The PET/CT imaging data was analyzed by using Pmod software (version 3.7, PMOD Technologies Ltd., Zurich, Switzerland). Seven volumes of interest (VOIs) for brain including caudate, putamen, thalamus, frontal cortex, occipital cortex, cerebellum, and whole brain were manually delineated on a T1-weighted MR image. An additional six VOIs for the noncentral nervous system including left ventricle, spleen, liver, spine, kidneys, and bladder were also manually delineated on the PET or CT image for whole body distribution. TACs were extracted from all the VOIs and expressed as percent injected dose per cm^3 (%ID/ cm^3) and SUV.

Metabolism Study. Blood analysis was conducted on venous samples collected at 5, 15, and 30 min postinjection. Whole blood and plasma activities were measured using a Wizard² 2480 gamma counter (PerkinElmer). Plasma samples were deproteinated by adding an equal volume of MeCN. The resulting plasma supernatant was then filtered through 0.45 μm Titan3 syringe filters (Thermo Scientific) and processed using a 1260 Infinity HPLC system (Agilent Technologies). The HPLC analysis utilized an Agilent Zorbax Eclipse XDB-C18 column (5 μm , 150×4.6 mm) with isocratic mobile phase of 73% TFA (0.1% v/v) and 27% MeCN, operating at a flow rate of 1.5 mL. Radioactivity was detected using a Posi-RAM radio-HPLC detector (LabLogic Systems). The Rt of the major polar metabolite was determined to be 1.3 min, while that of [^{11}C]4i was 6.1 min, which was confirmed by nonradioactive 4i.

■ ASSOCIATED CONTENT

Data Availability Statement

The article contains the complete data used to support the findings of this study.

Supporting Information

The Supporting Information is available free of charge at <https://pubs.acs.org/doi/10.1021/acs.jmedchem.3c00779>.

In vitro full competition curves of selected compounds 4f, 4g, 4i, 4j, 4k, 4m, and 4o–q, off-target binding profiles of 4i, Scatchard analysis of [^3H]4i in AD, PSP, and CBS, antibodies used in the immunohistochemistry studies, synthesis, characterization, and cross-linking of CLX4i, blocking studies of [^3H]4i with unlabeled compound, 4i in PD, MSA, and control brain sections, preparative and analytic HPLC chromatograms for radiosynthesis of [^{11}C]4i, BOILED-Egg plot of heterocyclic analogs, whole body PET images and TACs of [^{11}C]4i in NHP, purity of heterocyclic analogs, and ^1H and ^{13}C NMR spectra (PDF)

Molecular formula strings (CSV)

AUTHOR INFORMATION

Corresponding Author

Robert H. Mach – Department of Radiology, Perelman School of Medicine, University of Pennsylvania, Philadelphia, Pennsylvania 19104-6323, United States; orcid.org/0000-0002-7645-2869; Email: rmach@pennmedicine.upenn.edu

Authors

Ho Young Kim – Department of Radiology, Perelman School of Medicine, University of Pennsylvania, Philadelphia, Pennsylvania 19104-6323, United States; orcid.org/0000-0003-4391-9642

Wai Kit Chia – Department of Radiology, Perelman School of Medicine, University of Pennsylvania, Philadelphia, Pennsylvania 19104-6323, United States

Chia-Ju Hsieh – Department of Radiology, Perelman School of Medicine, University of Pennsylvania, Philadelphia, Pennsylvania 19104-6323, United States; orcid.org/0000-0002-2833-7727

Dinahlee Saturnino Guarino – Department of Radiology, Perelman School of Medicine, University of Pennsylvania, Philadelphia, Pennsylvania 19104-6323, United States

Thomas J. A. Graham – Department of Radiology, Perelman School of Medicine, University of Pennsylvania, Philadelphia, Pennsylvania 19104-6323, United States; orcid.org/0000-0002-3733-4106

Zsafia Lengyel-Zhand – Department of Radiology, Perelman School of Medicine, University of Pennsylvania, Philadelphia, Pennsylvania 19104-6323, United States

Mark Schneider – Department of Radiology, Perelman School of Medicine, University of Pennsylvania, Philadelphia, Pennsylvania 19104-6323, United States

Cosette Tomita – Department of Radiology, Perelman School of Medicine, University of Pennsylvania, Philadelphia, Pennsylvania 19104-6323, United States

Marshall G. Lougee – Department of Chemistry, University of Pennsylvania, Philadelphia, Pennsylvania 19104-6323, United States

Hee Jong Kim – Department of Biochemistry and Biophysics, Perelman School of Medicine, University of Pennsylvania, Philadelphia, Pennsylvania 19104-6303, United States

Vinayak V. Pagar – Department of Chemistry, University of Pennsylvania, Philadelphia, Pennsylvania 19104-6323, United States

Hsiaoju Lee – Department of Radiology, Perelman School of Medicine, University of Pennsylvania, Philadelphia, Pennsylvania 19104-6323, United States

Catherine Hou – Department of Radiology, Perelman School of Medicine, University of Pennsylvania, Philadelphia, Pennsylvania 19104-6323, United States; orcid.org/0000-0001-8905-8492

Benjamin A. Garcia – Department of Biochemistry and Biophysics, Perelman School of Medicine, University of Pennsylvania, Philadelphia, Pennsylvania 19104-6303, United States; orcid.org/0000-0002-2306-1207

E. James Petersson – Department of Chemistry, University of Pennsylvania, Philadelphia, Pennsylvania 19104-6323, United States

Jennifer O'Shea – Department of Neurology, Washington University School of Medicine, Saint Louis, Missouri 63110-1010, United States

Paul T. Kotzbauer – Department of Neurology, Washington University School of Medicine, Saint Louis, Missouri 63110-1010, United States

Chester A. Mathis – Department of Radiology, University of Pittsburgh, Pittsburgh, Pennsylvania 15213, United States

Virginia M.-Y. Lee – Center for Neurodegenerative Disease Research, Pathology and Laboratory Medicine, University of Pennsylvania, Philadelphia, Pennsylvania 19104-2676, United States

Kelvin C. Luk – Center for Neurodegenerative Disease Research, Pathology and Laboratory Medicine, University of Pennsylvania, Philadelphia, Pennsylvania 19104-2676, United States

Complete contact information is available at:

<https://pubs.acs.org/10.1021/acs.jmedchem.3c00779>

Funding

This work was supported by a grant from U19 NS110456. M.G.L. was supported by an Age Related Neurodegenerative Disease Training Grant fellowship (NIH T32-AG000255).

Notes

The authors declare the following competing financial interest(s): An invention disclosure has been filed on the compounds described in this paper.

ACKNOWLEDGMENTS

The authors would like to thank Mr. Anthony Young for performing the metabolite analysis studies. Human PD tissue samples were provided by Dr. Thomas Beach at the Banner Sun Health Research Institute and Body Donation Program of Sun City, AZ. This program is funded by NIH grant NS072026 and the Michael J. Fox Foundation. Human PSP and CBD tissue samples were provided by the Neurodegenerative Disease Brain Bank at the University of California, San Francisco, which receives funding support from NIH grants P30AG062422, P01AG019724, U01AG057195, and U19AG063911, the Rainwater Charitable Foundation, and the Bluefield Project to Cure FTD. Off-target binding profiles for GPCRs were generously provided by the National Institute of Mental Health's Psychoactive Drug Screening Program, Contract# HHSN-271-2018-00023-C (NIMH PDSP). The NIMH PDSP is Directed by Bryan L. Roth MD, PhD at the University of North Carolina at Chapel Hill and Project Officer Jamie Driscoll at NIMH, Bethesda MD, USA.

ABBREVIATIONS USED

Aq, aqueous; Boc, *tert*-butoxycarbonyl; CAA, cerebral amyloid angiopathy; DIPEA, *N,N*-diisopropylethylamine; DMF, dimethylformamide; DMSO, dimethyl sulfoxide; HPLC, high-performance liquid chromatography; MRI, magnetic resonance imaging; RT, room temperature; Rt, retention time; SD, standard deviation; TFA, trifluoroacetic acid; UHPLC, ultrahigh pressure liquid chromatography; UV, ultraviolet

REFERENCES

- (1) Skovronsky, D. M.; Lee, V. M.; Trojanowski, J. Q. Neurodegenerative diseases: new concepts of pathogenesis and their therapeutic implications. *Annu. Rev. Pathol.* **2006**, *1*, 151–70.
- (2) McCann, H.; Stevens, C. H.; Cartwright, H.; Halliday, G. M. alpha-Synucleinopathy phenotypes. *Parkinsonism Relat Disord* **2014**, *20*, S62–S67.
- (3) Yamasaki, T. R.; Holmes, B. B.; Furman, J. L.; Dhavale, D. D.; Su, B. W.; Song, E. S.; Cairns, N. J.; Kotzbauer, P. T.; Diamond, M. I.

Parkinson's disease and multiple system atrophy have distinct alpha-synuclein seed characteristics. *J. Biol. Chem.* **2019**, *294*, 1045–1058.

(4) Spillantini, M. G.; Crowther, R. A.; Jakes, R.; Hasegawa, M.; Goedert, M. alpha-Synuclein in filamentous inclusions of Lewy bodies from Parkinson's disease and dementia with lewy bodies. *Proc. Natl. Acad. Sci. U. S. A.* **1998**, *95*, 6469–73.

(5) Arima, K.; Ueda, K.; Sunohara, N.; Hirai, S.; Izumiya, Y.; Tonozuka-Uehara, H.; Kawai, M. Immunoelectron-microscopic demonstration of NACP/alpha-synuclein-epitopes on the filamentous component of Lewy bodies in Parkinson's disease and in dementia with Lewy bodies. *Brain Res.* **1998**, *808*, 93–100.

(6) Braak, H.; Sandmann-Keil, D.; Gai, W.; Braak, E. Extensive axonal Lewy neurites in Parkinson's disease: a novel pathological feature revealed by alpha-synuclein immunocytochemistry. *Neurosci. Lett.* **1999**, *265*, 67–9.

(7) Papp, M. I.; Kahn, J. E.; Lantos, P. L. Glial cytoplasmic inclusions in the CNS of patients with multiple system atrophy (striatonigral degeneration, olivopontocerebellar atrophy and Shy-Drager syndrome). *J. Neurol. Sci.* **1989**, *94*, 79–100.

(8) Woerman, A. L.; Watts, J. C.; Aoyagi, A.; Giles, K.; Middleton, L. T.; Prusiner, S. B. alpha-Synuclein: Multiple System Atrophy Prions. *Cold Spring Harb Perspect Med.* **2018**, *8*, a024588.

(9) Jellinger, K. A.; Lantos, P. L. Papp-Lantos inclusions and the pathogenesis of multiple system atrophy: an update. *Acta Neuropathol* **2010**, *119*, 657–67.

(10) Lengyel-Zhand, Z.; Ferrie, J. J.; Janssen, B.; Hsieh, C. J.; Graham, T.; Xu, K. Y.; Haney, C. M.; Lee, V. M.; Trojanowski, J. Q.; Petersson, E. J.; Mach, R. H. Synthesis and characterization of high affinity fluorogenic alpha-synuclein probes. *Chem. Commun. (Camb)* **2020**, *56*, 3567–3570.

(11) Alzghool, O. M.; van Dongen, G.; van de Giessen, E.; Schoonmade, L.; Beaino, W. alpha-Synuclein Radiotracer Development and In Vivo Imaging: Recent Advancements and New Perspectives. *Mov Disord* **2022**, *37*, 936–948.

(12) Peng, C.; Gathagan, R. J.; Covell, D. J.; Medellin, C.; Stieber, A.; Robinson, J. L.; Zhang, B.; Pitkin, R. M.; Olufemi, M. F.; Luk, K. C.; Trojanowski, J. Q.; Lee, V. M. Cellular milieu imparts distinct pathological alpha-synuclein strains in alpha-synucleinopathies. *Nature* **2018**, *557*, 558–563.

(13) Van der Perren, A.; Gelders, G.; Fenyi, A.; Bousset, L.; Brito, F.; Peelaerts, W.; Van den Haute, C.; Gentleman, S.; Melki, R.; Baekelandt, V. The structural differences between patient-derived alpha-synuclein strains dictate characteristics of Parkinson's disease, multiple system atrophy and dementia with Lewy bodies. *Acta Neuropathol* **2020**, *139*, 977–1000.

(14) Mattila, P. M.; Rinne, J. O.; Helenius, H.; Dickson, D. W.; Roytta, M. Alpha-synuclein-immunoreactive cortical Lewy bodies are associated with cognitive impairment in Parkinson's disease. *Acta Neuropathol* **2000**, *100*, 285–290.

(15) Kramer, M. L.; Schulz-Schaeffer, W. J. Presynaptic alpha-synuclein aggregates, not Lewy bodies, cause neurodegeneration in dementia with Lewy bodies. *J. Neurosci.* **2007**, *27*, 1405–10.

(16) Kotzbauer, P. T.; Cairns, N. J.; Campbell, M. C.; Willis, A. W.; Racette, B. A.; Tabbal, S. D.; Perlmutter, J. S. Pathologic accumulation of alpha-synuclein and Abeta in Parkinson disease patients with dementia. *Arch Neurol* **2012**, *69*, 1326–31.

(17) Klunk, W. E.; Engler, H.; Nordberg, A.; Wang, Y.; Blomqvist, G.; Holt, D. P.; Bergstrom, M.; Savitcheva, I.; Huang, G. F.; Estrada, S.; Ausen, B.; Debnath, M. L.; Barletta, J.; Price, J. C.; Sandell, J.; Lopresti, B. J.; Wall, A.; Koivisto, P.; Antoni, G.; Mathis, C. A.; Langstrom, B. Imaging brain amyloid in Alzheimer's disease with Pittsburgh Compound-B. *Ann. Neurol.* **2004**, *55*, 306–19.

(18) Wong, D. F.; Rosenberg, P. B.; Zhou, Y.; Kumar, A.; Raymond, V.; Ravert, H. T.; Dannals, R. F.; Nandi, A.; Brasic, J. R.; Ye, W.; Hilton, J.; Lyketos, C.; Kung, H. F.; Joshi, A. D.; Skovronsky, D. M.; Pontecorvo, M. J. In vivo imaging of amyloid deposition in Alzheimer disease using the radioligand 18F-AV-45 (florbetapir [corrected] F 18). *J. Nucl. Med.* **2010**, *51*, 913–20.

(19) Choi, S. R.; Schneider, J. A.; Bennett, D. A.; Beach, T. G.; Bedell, B. J.; Zehntner, S. P.; Krautkramer, M. J.; Kung, H. F.; Skovronsky, D. M.; Hefti, F.; Clark, C. M. Correlation of amyloid PET ligand florbetapir F 18 binding with Abeta aggregation and neuritic plaque deposition in postmortem brain tissue. *Alzheimer Dis Assoc Disord* **2012**, *26*, 8–16.

(20) Becker, G. A.; Ichise, M.; Barthel, H.; Luthardt, J.; Patt, M.; Seese, A.; Schultze-Mosgau, M.; Rohde, B.; Gertz, H. J.; Reiningner, C.; Sabri, O. PET quantification of 18F-florbetaben binding to beta-amyloid deposits in human brains. *J. Nucl. Med.* **2013**, *54*, 723–31.

(21) Chien, D. T.; Szardenings, A. K.; Bahri, S.; Walsh, J. C.; Mu, F.; Xia, C.; Shankle, W. R.; Lerner, A. J.; Su, M. Y.; Elizarov, A.; Kolb, H. C. Early clinical PET imaging results with the novel PHF-tau radioligand [F18]-T808. *J. Alzheimers Dis* **2013**, *38*, 171–84.

(22) Chiotis, K.; Saint-Aubert, L.; Savitcheva, I.; Jelic, V.; Andersen, P.; Jonasson, M.; Eriksson, J.; Lubberink, M.; Almkvist, O.; Wall, A.; Antoni, G.; Nordberg, A. Imaging in-vivo tau pathology in Alzheimer's disease with THK5317 PET in a multimodal paradigm. *Eur. J. Nucl. Med. Mol. Imaging* **2016**, *43*, 1686–99.

(23) Ono, M.; Sahara, N.; Kumata, K.; Ji, B.; Ni, R.; Koga, S.; Dickson, D. W.; Trojanowski, J. Q.; Lee, V. M.; Yoshida, M.; Hozumi, I.; Yoshiyama, Y.; van Swieten, J. C.; Nordberg, A.; Sahara, T.; Zhang, M. R.; Higuchi, M. Distinct binding of PET ligands PBB3 and AV-1451 to tau fibril strains in neurodegenerative tauopathies. *Brain* **2017**, *140*, 764–780.

(24) Beyer, L.; Brendel, M. Imaging of Tau Pathology in Neurodegenerative Diseases: An Update. *Semin Nucl. Med.* **2021**, *51*, 253–263.

(25) Jack, C. R., Jr.; Barrio, J. R.; Kepe, V. Cerebral amyloid PET imaging in Alzheimer's disease. *Acta Neuropathol* **2013**, *126*, 643–57.

(26) Capotosti, F.; Vokali, E.; Molette, J.; Ravache, M.; Delgado, C.; Kocher, J.; Pittet, L.; Vallet, C.; Serra, A.; Piorowska, K.; Dimitrakopoulos, I. K.; Luthi-Carter, R.; Tsika, E.; Touilloux, T.; Hliva, V.; Smith, R.; Hansson, O.; Streffer, J.; Pfeifer, A.; Kosco-Vilbois, M. Discovery of [18F]ACI-12589, a Novel and Promising PET-Tracer for Alpha-Synuclein. *Alzheimer's & Dementia* **2022**, *18*, e064680.

(27) Korat, S.; Bidesi, N. S. R.; Bonanno, F.; Di Nanni, A.; Hoang, A. N. N.; Herfert, K.; Maurer, A.; Battisti, U. M.; Bowden, G. D.; Thonon, D.; Vugts, D.; Windhorst, A. D.; Herth, M. M. Alpha-Synuclein PET Tracer Development-An Overview about Current Efforts. *Pharmaceuticals (Basel)* **2021**, *14*, 847.

(28) Bagchi, D. P.; Yu, L.; Perlmutter, J. S.; Xu, J.; Mach, R. H.; Tu, Z.; Kotzbauer, P. T. Binding of the radioligand SIL23 to alpha-synuclein fibrils in Parkinson disease brain tissue establishes feasibility and screening approaches for developing a Parkinson disease imaging agent. *PLoS One* **2013**, *8*, e55031.

(29) Mathis, C. A.; Lopresti, B. J.; Ikonovic, M. D.; Klunk, W. E. Small-molecule PET Tracers for Imaging Proteinopathies. *Semin Nucl. Med.* **2017**, *47*, 553–575.

(30) Tuttle, M. D.; Comellas, G.; Nieuwkoop, A. J.; Covell, D. J.; Berthold, D. A.; Klopper, K. D.; Courtney, J. M.; Kim, J. K.; Barclay, A. M.; Kendall, A.; Wan, W.; Stubbs, G.; Schwieters, C. D.; Lee, V. M.; George, J. M.; Rienstra, C. M. Solid-state NMR structure of a pathogenic fibril of full-length human alpha-synuclein. *Nat. Struct. Mol. Biol.* **2016**, *23*, 409–15.

(31) Chen, G. F.; Xu, T. H.; Yan, Y.; Zhou, Y. R.; Jiang, Y.; Melcher, K.; Xu, H. E. Amyloid beta: structure, biology and structure-based therapeutic development. *Acta Pharmacol Sin* **2017**, *38*, 1205–1235.

(32) Goedert, M.; Eisenberg, D. S.; Crowther, R. A. Propagation of Tau Aggregates and Neurodegeneration. *Annu. Rev. Neurosci.* **2017**, *40*, 189–210.

(33) Shah, M.; Seibyl, J.; Cartier, A.; Bhatt, R.; Catafau, A. M. Molecular imaging insights into neurodegeneration: focus on alpha-synuclein radiotracers. *J. Nucl. Med.* **2014**, *55*, 1397–400.

(34) Borroni, E.; Gobbi, L.; Honer, M.; Edelmann, M.; Mitchell, D.; Hardick, D.; Schmidt, W.; Steele, C.; Mulla, M. Radiolabeled compounds. *WO 2019/121661*, 2018.

(35) Hsieh, C. J.; Ferrie, J. J.; Xu, K.; Lee, I.; Graham, T. J. A.; Tu, Z.; Yu, J.; Dhavale, D.; Kotzbauer, P.; Petersson, E. J.; Mach, R. H. Alpha

Synuclein Fibrils Contain Multiple Binding Sites for Small Molecules. *ACS Chem. Neurosci.* **2018**, *9*, 2521–2527.

(36) Reilly, S. W.; Riad, A. A.; Hsieh, C. J.; Sahlholm, K.; Jacome, D. A.; Griffin, S.; Taylor, M.; Weng, C. C.; Xu, K.; Kirschner, N.; Luedtke, R. R.; Parry, C.; Malhotra, S.; Karanicolas, J.; Mach, R. H. Leveraging a Low-Affinity Diazaspiro Orthosteric Fragment to Reduce Dopamine D3 Receptor (D3R) Ligand Promiscuity across Highly Conserved Aminergic G-Protein-Coupled Receptors (GPCRs). *J. Med. Chem.* **2019**, *62*, 5132–5147.

(37) Hernandez, S.; Moreno, I.; SanMartin, R.; Herrero, M. T.; Dominguez, E. An straightforward entry to new pyrazolo-fused dibenzo[1,4]diazepines. *Org. Biomol. Chem.* **2011**, *9*, 2251–7.

(38) Kim, H. Y.; Lee, J. Y.; Hsieh, C. J.; Riad, A.; Izzo, N. J.; Catalano, S. M.; Graham, T. J. A.; Mach, R. H. Screening of sigma(2) Receptor Ligands and In Vivo Evaluation of (11)C-Labeled 6,7-Dimethoxy-2-[4-(4-methoxyphenyl)butan-2-yl]-1,2,3,4-tetrahydroisoquinoline for Potential Use as a sigma(2) Receptor Brain PET Tracer. *J. Med. Chem.* **2022**, *65*, 6261–6272.

(39) Xu, K.; Hsieh, C. J.; Lee, J. Y.; Riad, A.; Izzo, N. J.; Look, G.; Catalano, S.; Mach, R. H. Exploration of Diazaspiro Cores as Piperazine Bioisosteres in the Development of sigma2 Receptor Ligands. *Int. J. Mol. Sci.* **2022**, *23*, 8259.

(40) Besnard, J.; Ruda, G. F.; Setola, V.; Abecassis, K.; Rodriguiz, R. M.; Huang, X. P.; Norval, S.; Sassano, M. F.; Shin, A. I.; Webster, L. A.; Simeons, F. R.; Stojanovski, L.; Prat, A.; Seidah, N. G.; Constam, D. B.; Bickerton, G. R.; Read, K. D.; Wetsel, W. C.; Gilbert, I. H.; Roth, B. L.; Hopkins, A. L. Automated design of ligands to polypharmacological profiles. *Nature* **2012**, *492*, 215–20.

(41) Ferrie, J. J.; Lengyel-Zhand, Z.; Janssen, B.; Lougee, M. G.; Giannakoulis, S.; Hsieh, C. J.; Pagar, V. V.; Weng, C. C.; Xu, H.; Graham, T. J. A.; Lee, V. M.; Mach, R. H.; Petersson, E. J. Identification of a nanomolar affinity alpha-synuclein fibril imaging probe by ultra-high throughput in silico screening. *Chem. Sci.* **2020**, *11*, 12746–12754.

(42) Janssen, B.; Tian, G.; Lengyel-Zhand, Z.; Hsieh, C. J.; Lougee, M. G.; Riad, A.; Xu, K.; Hou, C.; Weng, C. C.; Lopresti, B. J.; Kim, H. J.; Pagar, V. V.; Ferrie, J. J.; Garcia, B. A.; Mathis, C. A.; Luk, K.; Petersson, E. J.; Mach, R. H. Identification of a Putative alpha-synuclein Radioligand Using an in silico Similarity Search. *Mol. Imaging Biol.* **2023**, *25*, 704.

(43) Strohaker, T.; Jung, B. C.; Liou, S. H.; Fernandez, C. O.; Riedel, D.; Becker, S.; Halliday, G. M.; Bennati, M.; Kim, W. S.; Lee, S. J.; Zweckstetter, M. Structural heterogeneity of alpha-synuclein fibrils amplified from patient brain extracts. *Nat. Commun.* **2019**, *10*, 5535.

(44) Daina, A.; Zoete, V. A BOILED-Egg To Predict Gastrointestinal Absorption and Brain Penetration of Small Molecules. *ChemMedChem.* **2016**, *11*, 1117–21.

(45) Daina, A.; Michielin, O.; Zoete, V. SwissADME: a free web tool to evaluate pharmacokinetics, drug-likeness and medicinal chemistry friendliness of small molecules. *Sci. Rep.* **2017**, *7*, 42717.

(46) Wildman, S. A.; Crippen, G. M. Prediction of Physicochemical Parameters by Atomic Contributions. *J. Chem. Inf. Comput. Sci.* **1999**, *39*, 868–873.

(47) Fellner, L.; Stefanova, N. The role of glia in alpha-synucleinopathies. *Mol. Neurobiol.* **2013**, *47*, 575–86.

(48) Xu, M. M.; Ryan, P.; Rudrawar, S.; Quinn, R. J.; Zhang, H. Y.; Mellick, G. D. Advances in the development of imaging probes and aggregation inhibitors for alpha-synuclein. *Acta Pharmacol Sin.* **2020**, *41*, 483–498.

(49) Chu, W.; Zhou, D.; Gaba, V.; Liu, J.; Li, S.; Peng, X.; Xu, J.; Dhavale, D.; Bagchi, D. P.; d'Avignon, A.; Shakerdge, N. B.; Bacskai, B. J.; Tu, Z.; Kotzbauer, P. T.; Mach, R. H. Design, Synthesis, and Characterization of 3-(Benzylidene)indolin-2-one Derivatives as Ligands for alpha-Synuclein Fibrils. *J. Med. Chem.* **2015**, *58*, 6002–17.

(50) Reilly, S. W.; Puentes, L. N.; Hsieh, C. J.; Makvandi, M.; Mach, R. H. Altering Nitrogen Heterocycles of AZD2461 Affords High Affinity Poly(ADP-ribose) Polymerase-1 Inhibitors with Decreased P-Glycoprotein Interactions. *ACS Omega* **2018**, *3*, 9997–10001.

(51) Pancoe, S. X.; Wang, Y. J.; Shimogawa, M.; Perez, R. M.; Giannakoulis, S.; Petersson, E. J. Effects of Mutations and Post-

Translational Modifications on alpha-Synuclein In Vitro Aggregation. *J. Mol. Biol.* **2022**, *434*, 167859.

(52) Anderson, C. J.; Walker, D. E.; Goldstein, J. M.; de Laat, R.; Banducci, K.; Caccavello, R. J.; Barbour, R.; Huang, J.; Kling, K.; Lee, M.; Diep, L.; Keim, P. S.; Shen, X.; Chataway, T.; Schlossmacher, M. G.; Seubert, P.; Schenk, D.; Sinha, S.; Gai, W. P.; Chilcote, T. J. Phosphorylation of Ser-129 is the dominant pathological modification of alpha-synuclein in familial and sporadic Lewy body disease. *J. Biol. Chem.* **2006**, *281*, 29739–52.

(53) Sonustun, B.; Altay, M. F.; Strand, C.; Ebanks, K.; Hondhamuni, G.; Warner, T. T.; Lashuel, H. A.; Bandopadhyay, R. Pathological Relevance of Post-Translationally Modified Alpha-Synuclein (pSer87, pSer129, nTyr39) in Idiopathic Parkinson's Disease and Multiple System Atrophy. *Cells* **2022**, *11*, 906.

(54) Zhang, S.; Zhu, R.; Pan, B.; Xu, H.; Olufemi, M. F.; Gathagan, R. J.; Li, Y.; Zhang, L.; Zhang, J.; Xiang, W.; Kagan, E. M.; Cao, X.; Yuan, C.; Kim, S. J.; Williams, C. K.; Magaki, S.; Vinters, H. V.; Lashuel, H. A.; Garcia, B. A.; James Petersson, E.; Trojanowski, J. Q.; Lee, V. M.; Peng, C. Post-translational modifications of soluble alpha-synuclein regulate the amplification of pathological alpha-synuclein. *Nat. Neurosci.* **2023**, *26*, 213–225.

(55) Hsieh, C. J.; Xu, K.; Lee, I.; Graham, T. J. A.; Tu, Z.; Dhavale, D.; Kotzbauer, P.; Mach, R. H. Chalcones and Five-Membered Heterocyclic Isosteres Bind to Alpha Synuclein Fibrils in Vitro. *ACS Omega* **2018**, *3*, 4486–4493.

(56) Klunk, W. E.; Wang, Y.; Huang, G. F.; Debnath, M. L.; Holt, D. P.; Shao, L.; Hamilton, R. L.; Ikonovic, M. D.; DeKosky, S. T.; Mathis, C. A. The binding of 2-(4'-methylaminophenyl)benzothiazole to postmortem brain homogenates is dominated by the amyloid component. *J. Neurosci.* **2003**, *23*, 2086–92.

(57) Klunk, W. E.; Wang, Y.; Huang, G. F.; Debnath, M. L.; Holt, D. P.; Mathis, C. A. Uncharged thioflavin-T derivatives bind to amyloid-beta protein with high affinity and readily enter the brain. *Life Sci.* **2001**, *69*, 1471–84.

(58) Pantel, A. R.; Viswanath, V.; Daube-Witherspoon, M. E.; Dubroff, J. G.; Muehlechner, G.; Parma, M. J.; Pryma, D. A.; Schubert, E. K.; Mankoff, D. A.; Karp, J. S. PennPET Explorer: Human Imaging on a Whole-Body Imager. *J. Nucl. Med.* **2020**, *61*, 144–151.